

Detecting Detached Black Hole binaries through Photometric Variability

CHIRAG CHAWLA,¹ SOURAV CHATTERJEE,¹ NEEV SHAH,² AND KATELYN BREIVIK³

¹*Tata Institute of Fundamental Research, Department of Astronomy and Astrophysics, Homi Bhabha Road, Navy Nagar, Colaba, Mumbai, 400005, India*

²*Indian Institute of Science Education and Research Pune, Dr. Homi Bhabha Road, Pune 411008, India*

³*Department of Physics, McWilliams Center for Cosmology and Astrophysics, Carnegie Mellon University, 5000 Forbes Avenue, Pittsburgh, PA 15213, USA*

ABSTRACT

Understanding the connection between the properties of black holes (BHs) and their progenitors is interesting in many branches of astrophysics. Discovering BHs in detached orbits with luminous companions (LCs) promises to help create this map since the LC and BH progenitor are expected to have the same metallicity and formation time. We explore the possibility of detecting BH–LC binaries in detached orbits using photometric variations of the LC flux, induced by tidal ellipsoidal variation, relativistic beaming, and self-lensing. We create realistic present-day populations of detached BH–LC binaries in the Milky Way (MW) using binary population synthesis where we adopt observationally motivated initial stellar and binary properties, star formation history and present-day distribution of these sources in the MW based on detailed cosmological simulations. We test detectability of these sources via photometric variability by *Gaia* and TESS missions by incorporating their respective detailed detection biases as well as interstellar extinction. We find that *Gaia* is expected to resolve $\sim 300\text{--}1,000$ ($\sim 700\text{--}1,500$) detached BH–LC binaries with $\text{SNR} \geq 10$ (1) depending on the photometric precision and details of supernova physics. Similarly, the number of resolved BH–LC binaries with TESS are $\sim 50\text{--}200$ ($\sim 140\text{--}350$). We find that 136^{+15}_{-15} BH–LC binaries would be common between *Gaia* and TESS. Moreover, between $\sim 60\text{--}70$ ($\sim 50\text{--}200$) BH–LC binaries identifiable using photometry with $\text{SNR} \geq 10$ may also be resolved using *Gaia*’s radial velocity (astrometry).

1. INTRODUCTION

Recent observations of merging double compact object (CO) binaries by the LIGO-Virgo-KAGRA (LVK) detectors have reignited the interest to understand the astrophysical origins of CO binaries (Abbott et al. 2016a,b, 2019; Abbott et al. 2021a,b). A variety of ongoing and upcoming missions including the Zwicky Transient Facility (ZTF, Bellm et al. 2018), the Rubin Observatory’s Legacy Survey of Space and Time (LSST, Ivezić et al. 2019), the All-Sky Automated Survey for Supernova (ASAS-SN, Shappee et al. 2014; Kochanek et al. 2017), SDSS-V (Kollmeier et al. 2017) and eROSITA (Predehl et al. 2021) are expected to unravel hundreds to thousands of COs including Cataclysmic variables, Supernova explosions, Gamma-ray bursts, and X-ray binaries.

Although understanding the demographics of dark remnants in general, and BHs in particular, is interesting for many branches of astrophysics, a model independent map connecting BHs to their stellar progenitors remains elusive due to challenges in the detailed theoretical modeling of the supernova physics (Patton & Sukhbold 2020; Patton et al. 2022; Fryer et al. 2022) and scarcity of discovered BHs where constraints to the progenitor properties are available (e.g., Breivik et al. 2019; El-Badry et al. 2022e).

BH–LC binaries in detached orbits, discovered in large numbers, can be instrumental in improving this gap in our understanding of the details of how high-mass stars evolve, explode, and form COs (Breivik et al. 2017; Chawla et al. 2022; Shikauchi et al. 2023). In particular, if the distance to the LC is known (e.g., via *Gaia* astrometry), meaningful constraints can be placed on the metallicity and age of the LC (and thus the BH’s progenitor) through stellar evolution models, asteroseismology, and spectroscopy (e.g. Lin et al. 2018; Angus

et al. 2019; Bellinger, E. P. et al. 2019). It is expected that $\sim 10^8 - 10^9$ stellar-mass BHs are present in the present-day MW (Brown & Bethe 1994; Olejak, A. et al. 2020; Sweeney et al. 2022). Of these, roughly $10^4 - 10^5$ are expected to be in binaries with a non-BH. An overwhelming 70 – 98% of BH–LC binaries are expected to have the LC in a detached orbit. In contrast, BHs in potentially mass transferring systems is only 2 – 30% (Breivik et al. 2017; Wiktorowicz et al. 2019; Chawla et al. 2022). Recent advances in time-domain astronomy promises to provide unprecedented constraints on BHs in detached orbits via high-precision astrometric, photometric, and spectroscopic measurements. BHs can be characterized using several techniques: (a) astrometrically constraining the orbit of a LC by observing its motion around an unseen primary (van de Kamp 1975; Gould & Salim 2002; Tomsick & Muterspaugh 2010), (b) spectroscopically measuring the RV of the LC as it moves around the BH (Zeldovich & Guseynov 1966; Trimble & Thorne 1969), and (c) phase-curve analysis of orbital photometric modulations of the LC induced by its dark companion (Shakura & Postnov 1987; Khruzina et al. 1988). Of course, at least for some sources, a combination of more than one of the above methods may become useful.

The prospect of detecting BHs in detached BH–LC binaries via ongoing astrometry and RV surveys like *Gaia* and LAMOST has been extensively explored (Barstow et al. 2014; Breivik et al. 2017; Mashian & Loeb 2017; Chawla et al. 2022; Janssens et al. 2022). Although the estimated number of detectable BH–LC binaries is model dependent (because of model uncertainties, e.g., in SNe physics), all of these studies predict that *Gaia* could possibly discover $10 - 10^3$ BH–LC binaries in detached orbits during its 10 year mission. In addition, the knowledge of the stellar parameters like luminosity, age, and mass of the LC can help constrain the mass of the BH as well as its progenitor’s properties in a model independent way (Fuchs & Bastian 2005; Andrews et al. 2019; Shahaf et al. 2019; Chawla et al. 2022).

Several non-interacting BH–LC candidates have been discovered in star clusters (Giesers et al. 2018; Giesers et al. 2019) and in the Large Magellanic Cloud (Shenar et al. 2022a; Lennon, D. J. et al. 2022; Saracino et al. 2021; Shenar et al. 2022b). In the Galactic field also, several discoveries of candidate BH–LC binaries in detached orbits, including BHs in triples, have been proposed by studies using photometric and spectroscopic observations (Qian et al. 2008; Casares et al. 2014; Khokhlov et al. 2018; Liu et al. 2019; Thompson et al. 2019; Rivinius, Th. et al. 2020; Gomez & Grindlay 2021; Jayasinghe et al. 2021). However, significant debate

persists on the candidature of many of these systems (e.g., it has been suggested that the unseen companion may actually be a low-luminosity sub-giant companion or stellar binary instead of a BH in some of the candidate systems; van den Heuvel & Tauris 2020; El-Badry & Quataert 2021; El-Badry & Burdge 2022; El-Badry et al. 2022a,b).

Most recently, using *Gaia*’s DR3 several groups have reported a number of possible dormant CO–LC candidate binaries using astrometry (Andrews et al. 2022; Gaia Collaboration et al. 2023; Chakrabarti et al. 2023; El-Badry et al. 2022e, 2023; Shahaf et al. 2022), photometry (Gomel, R. et al. 2023) and spectroscopy (Fu et al. 2022; Jayasinghe et al. 2023; Nagarajan et al. 2023; Tanikawa et al. 2023; Zhao et al. 2023), which indicates that indeed a large population of BH–LC binaries in detached orbits do exist in nature and are waiting to be found.

Observations of photometric variability in stars due to planetary transits have revolutionized the field by detecting thousands of exoplanets from various wide-field ground-based missions including HAT (Bakos et al. 2004), TrES (Alonso et al. 2004), XO (McCullough et al. 2005), WASP (Pollacco et al. 2006) and KELT (Pepper et al. 2007) and space missions like CoRoT (Auvergne, M. et al. 2009), *Kepler* (Borucki et al. 2011), and TESS (Ricker et al. 2014). Periodic variability in the observed LC flux is also expected in compact orbits around BHs. For example, in a compact enough orbit to a BH, the sky-projected surface area of an LC may show orbital phase-dependent changes resulting in the so-called ellipsoidal variations (EV) in the total observed flux. In addition, relativistic beaming (RB) of the LC’s light may be strong enough to be detectable if its orbit is close-enough to a BH. Furthermore, if the geometry is favorable, light from the LC may be lensed by the BH, and the magnification due to this self-lensing (SL) within the binaries may be large enough to be detectable. Stellar binaries have already been detected using such photometric variations both in eclipsing and non-eclipsing configurations (Morris 1985; Thompson et al. 2012; Herrero, E. et al. 2014; Nie et al. 2017). While microlensing surveys such as OGLE and MACHO have reported a number of isolated compact object candidates (Abdurrahman et al. 2021; Lam et al. 2022; Mróz et al. 2022; Sahu et al. 2022), detection of compact objects in orbit around an LC remains illusive. Nevertheless, recent theoretical studies estimate that a significant number of detached BH–LC binaries ($\sim 10 - 100$) may be observed by phase-curve analysis of their LCs with ongoing photometric surveys such as TESS, ZTF, LSST and *Kepler*

(Masuda & Hotokezaka 2019; Gomel et al. 2020; Wiktorowicz et al. 2021; Hu et al. 2023).

Using our realistic simulated Galactic populations of BH–LC binaries presented in the context of *Gaia*’s astrometric detectability (Chawla et al. 2022, hereafter Paper I), we investigate the ability of *Gaia* and TESS to resolve detached BH–LCs via photometric orbital modulation induced through tidal and relativistic effects. A similar analysis for LSST would also be very interesting, however, a realistic analysis for signal to noise ratio (SNR) is not straightforward for LSST at this time. We discuss the details of our simulated models in section 2. In section 3 we describe how we calculate SNR taking into account the detection biases and our adopted detection criteria. In section 4 we present our key results for the intrinsic as well as detectable BH–LCs. We discuss possibilities from follow-up studies in section 5 and conclude in section 7.

2. NUMERICAL METHODS

The synthetic populations used in this study are described in detail in Paper I. Nevertheless, we present the crucial details relevant for this study for completeness. We create representative present-day BH–LC populations using the state-of-art Python-based rapid binary population synthesis (BPS) suite COSMIC (Breivik et al. 2020) which employs the SSE/BSE evolutionary framework to evolve single and binary stars (Hurley et al. 2000; Hurley et al. 2002).

Using COSMIC we generate a population of zero-age main sequence (ZAMS) binaries by assigning initial ages, metallicities (Z), masses, semimajor axes (a), and eccentricities (Ecc). The initial age and metallicity of each binary is sampled from the final snapshot of the **m12i** model galaxy from the Latte suite of the Feedback In Realistic Environments (FIRE-2) simulations (Wetzel et al. 2016; Hopkins et al. 2018). The single-star stellar evolution tracks used in COSMIC only incorporate metallicities in the range $\log(Z/Z_\odot) = -2.3$ and 0.2 , where $Z_\odot = 0.02$ is the solar metallicity. Hence, we confine the metallicities of our simulated binaries within this range and assign the limiting values for metallicities in **m12i** which are outside this range.

The stellar and orbital parameters for the ZAMS population such as mass, orbital period (P_{orb}), Ecc and mass ratio ($q \leq 1$) are sampled from observationally motivated probability distribution functions. The primary mass is sampled from the Kroupa (2001) initial stellar mass function (IMF) between $M_{\text{min}}/M_\odot = 0.08$ and $M_{\text{max}}/M_\odot = 150$ and the secondary mass is assigned in the range M_{min} to the primary mass using a flat q distribution (Mazeh et al. 1992; Goldberg &

Mazeh 1994). We assume initially thermal Ecc distribution (e.g., Jeans 1919; Ambartsumian 1937; Heggie 1975). The initial a are drawn to be uniform in log with an upper bound of $10^5 R_\odot$ and inner bound such that $R_{\text{pri}} \leq R_{\text{RL}}/2$ (Han 1998), where R_{pri} is the radius of the primary component and R_{RL} is its Roche radius.

COSMIC uses several modified prescriptions beyond the standard BSE implementations described in Hurley et al. (2002) to evolve the binary population from ZAMS to get the present-day BH–LC population in the MW. For a detailed description of these modifications see Breivik et al. (2020). The properties of the present day BH–LC binary population depends strongly on the outcome of the Roche-overflow mass transfer from the BH progenitor and the natal kick imparted during BH formation. We adopt critical mass ratios as a function of donor type derived from the adiabatic response of the donor radius and its Roche radius (Belczynski et al. 2008) to determine whether mass transfer remains dynamically stable or leads to a common envelope (CE) evolution (Webbink 1985).

For CE evolution COSMIC uses a formulation based on the orbital energy; the CE is parameterized using two parameters α (Livio & Soker 1984) and λ where, α denotes the efficiency of using the orbital energy to eject the envelope and λ defines the binding energy of the envelope based on the donor’s stellar structure (Tout et al. 1997). We adopt $\alpha = 1$ and that λ depends on the evolutionary phase of the donor (see Appendix A of Claeys et al. 2014). We adopt two widely used explosion mechanisms for BH formation via core-collapse supernovae (CCSNe): “rapid” and “delayed” (Fryer et al. 2012). While these two prescriptions introduce several differences in the BHs’ birth mass function and natal kicks, the most prominent for our study is the presence (absence) of a mass gap between (3 and 5 M_\odot) NSs and BHs produced via core-collapse SNe (CCSNe) in the rapid (delayed) prescription. We refer to the model populations created using the rapid (delayed) prescription as **rapid** (**delayed**) model. We assign BH natal kicks with magnitude $v(1 - f_{\text{FB}})$, where v is drawn from a Maxwellian distribution with $\sigma = 265$ (Hobbs et al. 2005) and f_{FB} is the fraction of mass fallback from the outer envelope of the exploding star (e.g. Belczynski et al. 2008).

2.1. Synthetic Milky-Way population

Using COSMIC, we evolve binaries until the distribution of present-day properties for BH–LC binaries saturate to a high degree of accuracy (for a more detailed description see Paper I). Typically, while creating this representative population we only simulate the evolu-

tion of a fraction of the total MW mass as defined by galaxy **m12i**. In order to obtain the correct number of BH-LC binaries in the MW at present, we up-scale the simulated BH-LC population by a factor proportional to the ratio of the entire stellar mass of **m12i** ($M_{\mathbf{m12i}}$) and the total simulated single and binary stellar mass (M_{sim}) in COSMIC.¹ The total number of the present-day BH-LC binaries in the MW is then defined as

$$N_{\text{BH-LC,MW}} = N_{\text{BH-LC,sim}} \frac{M_{\mathbf{m12i}}}{M_{\text{sim}}}. \quad (1)$$

To produce a MW-representative population of present-day BH-LC binaries, we sample (with replacement) $N_{\text{BH-LC,MW}}$ binaries from our simulated population of BH-LC binaries to assign a complete set of stellar and orbital parameters including mass, metallicity, luminosity, radius, eccentricity, and P_{orb} . Each binary is also assigned a Galactocentric position by locating the star-particle closest to the given binary in age and metallicity in the **m12i** galaxy model with an offset following the Ananke framework (Sanderson et al. 2020). Hence, we preserve the complex correlations between Galactic location, metallicity, and stellar density in the MW. Finally, each binary is assigned a random orientation by specifying the Campbell elements, inclination (i) with respect to the line of sight, argument of periapsis (ω) and longitude of ascending node (Ω). We create 200 MW realizations for each model (**rapid** and **delayed**) to investigate the variance associated with the random assignments of each binary in the procedure described above.

We incorporate the effect of interstellar extinction and reddening by calculating extinction (A_v) using the python package `mw dust` (Drimmel et al. 2003; Marshall et al. 2006; Bovy et al. 2016; Green et al. 2019) based on the position of binaries in the galaxy and include this correction in estimating the TESS and *Gaia* magnitudes.

3. PHOTOMETRIC VARIABILITY AND DETECTION

TESS and *Gaia* are both all-sky surveys despite different primary observing goals and strategies. For both, the number and epochs of observations of any particular source over the full mission duration are dependent on its Galactic coordinates. We consider three physical processes which can introduce orbital modulation in the LC's observed flux: ellipsoidal variation due to tidal distortion of the LC (EV), relativistic beaming (RB), and

self-lensing (SL). Below we describe how we estimate the signal to noise ratio in TESS and *Gaia* photometry and our detectability conditions.

3.1. SNR calculation

The relevant SNR for TESS observation for a source undergoing photometric variations can be written as (Sullivan et al. 2015)

$$[S/N]_{\text{TESS}} = \frac{\sqrt{\frac{1}{2\pi} \int \left(\frac{\Delta \mathcal{F}}{\langle \mathcal{F} \rangle} \right)^2 d\phi}}{\sigma_{30}/\sqrt{N}}. \quad (2)$$

$\Delta \mathcal{F} \equiv \mathcal{F}(\phi) - \langle \mathcal{F} \rangle$, where $\langle \mathcal{F} \rangle$ is the orbital phase ϕ -averaged flux, σ_{30} is the per-point combined differential photometric precision of TESS with 30-minute cadence. σ_{30} depends on the source's reddening corrected TESS magnitude and calculated using the python package `ticgen` (Barclay 2017; Stassun et al. 2018). N is the number of photometric data points with 30-minute cadence for the source given its Galactic location using the tool, `tess-point` (Burke et al. 2020). Similarly, for *Gaia* we define the SNR as

$$[S/N]_{\text{Gaia}} = \frac{\sqrt{\frac{1}{2\pi} \int (\Delta G(\phi))^2 d\phi}}{\sigma_G/\sqrt{N}}, \quad (3)$$

where $\Delta G \equiv G(\phi) - \langle G \rangle$, where $\langle G \rangle$ is ϕ -averaged *Gaia* magnitude. $G(\phi)$ is calculated from $\mathcal{F}(\phi)$ and effective temperature (T). σ_G is the photometric precision of *Gaia* with 8 – 10 sec cadence and depends on G .² N is the location-dependent number of data points obtained during *Gaia*'s 10-year observation estimated for each source using *Gaia*'s Observation Forecast Tool (GOST).³ The magnitudes for the photometric variability of course depend on the physical process responsible. Note that the noise modelling is based on the power-law fitting. Other factors such as stellar crowding could also contribute to the SNR and hence detections. However, including a crowding model in this study would require the information of field stars from other observational catalogs which is far from the scope of this study. Also while estimating the SNR of the SL signal, an alternative approach could be to do a summation on the integrals (Equation 2,3) on representative cadences for the mission in consideration.

3.1.1. Ellipsoidal Variation

¹ We do not simulate single stars. Instead we adopt an observationally motivated binary fraction (Duchêne & Kraus 2013; Moe & Stefano 2017) to estimate the equivalent total mass from the simulated binary mass.

² The slight difference between the SNR expressions stems from the differences in the dimensions of reported σ_{30} and σ_G .

³ <https://gaia.esac.esa.int/gost/>

The tidal force of the BH distorts the shape of the LC, elongating it along the line joining the center of the BH–LC system. The surface flux distribution also changes due to gravity darkening (Zeipel 1924; Kopal 1959). Due to the orbital motion of the LC, its net sky-projected area varies resulting in a periodic modulation of the observed flux. The observed flux as a function of phase (ϕ) due to EV is (Morris & Naftilan 1993)-

$$\begin{aligned} \mathcal{F}(\phi) = & \mathcal{F}_0 \left[1 + \left(\frac{\alpha}{9} \right) \left(\frac{R_{\text{LC}}}{a} \right)^3 (2 + 2q)(2 - 3 \sin^2 i) \right. \\ & + \left(\frac{\alpha}{9} \right) \frac{1 + e \cos \phi}{1 - e^2} \left(\frac{R_{\text{LC}}}{a} \right)^3 (3q)(2 - 3 \sin^2 i) \\ & \left. - (\alpha) \frac{1 + e \cos \phi}{1 - e^2} \left(\frac{R_{\text{LC}}}{a} \right)^3 (q)(\sin^2 i)(\cos(2\omega + 2\phi - \pi)) \right], \end{aligned} \quad (4)$$

where, $\mathcal{F}(\phi)$ represents the Flux of the LC as a function of the orbital phase (ϕ), \mathcal{F}_0 denotes the luminosity in the absence of the BH, and α is defined as

$$\alpha = \frac{15u(2 + \tau)}{32(3 - u)}, \quad (5)$$

where u and τ are the limb and gravity darkening coefficients, respectively (Morris & Naftilan 1993; Engel et al. 2020). For simplicity, we ignore the contribution from limb and gravity darkening in this study (i.e., $u = 0.3$, $\tau = 0.4$, $\alpha = 0.125$) since they are expected to have a small effect on the overall results.

3.1.2. Relativistic Beaming

The photometric modulation due to the relative motion between the LC and the observer is known as relativistic beaming. The radial component of the orbital motion of the LC induced by the BH causes a phase-dependent flux variation due to relativistic effects, such as the doppler effect, time dilation, and aberration of light (van Kerkwijk et al. 2010; Bloemen et al. 2011). The amplitude of the photometric variation resulting from beaming is proportional to the radial velocity semi-amplitude of the LC (K_{LC}), and can be expressed as (Loeb & Gaudi 2003)

$$\begin{aligned} \frac{\Delta \mathcal{F}}{\langle \mathcal{F} \rangle} = & 4\alpha_{\text{RB}} \frac{K_{\text{LC}}}{c} \\ = & 2830 \alpha_{\text{RB}} \sin i \left(\frac{P_{\text{orb}}}{\text{days}} \right)^{-1/3} \\ & \times \left(\frac{M_{\text{BH}} + M_{\text{LC}}}{M_{\odot}} \right)^{-2/3} \left(\frac{M_{\text{BH}}}{M_{\odot}} \right), \end{aligned} \quad (6)$$

where, α_{RB} is obtained by integrating the frequency-dependent term

$$\alpha_{\text{RB},\nu} = \frac{1}{4} \left(3 - \frac{d \ln \mathcal{F}_{\nu}}{d \ln \nu} \right) \quad (7)$$

over the frequency range of the band-pass (Loeb & Gaudi 2003). The value of bolometric $\alpha_{\text{RB}} = 1$ and it deviates from 1 while considering only a bandpass of wavelength range (Loeb & Gaudi 2003; Zucker et al. 2007). In the black-body approximation for a wide range of surface temperatures the value of α_{RB} remains close to 1 (Shporer 2017). In this study, we have assumed $\alpha_{\text{RB}} \approx 1$ for simplicity.

3.1.3. Self Lensing

For BH–LC binaries with orbits aligned with the line-of-sight, the BH acts as a lens magnifying the LC thus producing a sudden shift in its luminosity during occultation. This generates a periodic spike or self-lensing signal every time the BH eclipses its companion (Leibovitz & Hube 1971; Maeder 1973; Gould 1995; Rahvar et al. 2010). The amplitude of the modulation in the light-curve depends on the magnification factor which is a function of binary separation, BH mass, and the inclination of the binary orbit with respect to the sky plane. The amplitude of the SL signal is adopted from Witt & Mao (1994) as

$$\mu_{\text{SL}} = \frac{1}{\pi} [c_F F(k) + c_E E(k) + c_{\Pi} \Pi(n, k)] \quad (8)$$

where F , E , and Π are complete elliptic integrals of first, second and third kind and the coefficients c_F , c_E , and c_{Π} are defined as

$$\begin{aligned} c_F = & -\frac{b-r}{r^2} \frac{4 + (b^2 - r^2)/2}{\sqrt{4 + (b-r)^2}} \\ c_E = & \frac{b+r}{2r^2} \sqrt{4 + (b-r)^2} \\ c_{\Pi} = & \frac{2(b-r)^2}{r^2(b+r)} \frac{1+r^2}{\sqrt{4 + (b-r)^2}} \\ n = & \frac{4br}{(b+r)^2} \\ k = & \sqrt{\frac{4n}{4 + (b-r)^2}}, \end{aligned} \quad (9)$$

where, the impact parameter

$$b = \frac{a \cos(i)}{R_E} \frac{1 - e^2}{1 + e \cos(f - \omega)}. \quad (10)$$

Here,

$$f = \tan^{-1} \left(\frac{1}{\tan \Omega \cos i} \right), \quad (11)$$

and r is the ratio of the LC radius and the BH's Einstein radius, R_{LC}/R_E . The Einstein radius

$$R_E = \sqrt{\frac{4GM_{\text{BH}}}{c^2} \frac{D_{\text{LS}} D_{\text{L}}}{D_{\text{S}}}} \quad (12)$$

where, D_{LS} , D_{L} , and D_{S} are the source-lens, lens-observer, and source-observer distances, respectively. For SL, $D_{\text{L}} \approx D_{\text{S}}$ and D_{LS} is given as;

$$D_{\text{LS}} = a \sin(i) \frac{1 - e^2}{1 + e \cos(f - \omega)}. \quad (13)$$

The SNR of the SL signal is defined as

$$\frac{\Delta \mathcal{F}}{\langle \mathcal{F} \rangle} = \mu_{\text{SL}} - 1 \quad (14)$$

where μ_{SL} is the magnification factor by which brightness of LC is modified during eclipses.

3.2. Detection criteria

We employ three necessary conditions to determine the detectability of a particular detached BH–LC binary through photometric variations either using *Gaia* or TESS:

1. $\text{SNR} \geq 10$.
2. The average apparent magnitude of the LC G ($m_{\text{LC}} \leq 20$ (25)), the limiting magnitudes for *Gaia* (TESS).
3. At least one full orbit of the BH–LC binary must be observed. For TESS, this condition can be expressed as $P_{\text{orb}} \leq t_{\text{dur}}$, where t_{dur} is the duration of observation given the Galactic coordinates of the source. For *Gaia* we consider the full extended mission duration of 10 years by imposing $P_{\text{orb}}/\text{yr} \leq 10$.

We call the subset of BH–LC binaries in each of our MW realisations that satisfy the above conditions as the ‘optimistic’ set for detectable BH–LC binaries. Essentially, this is a collection of sources that are resolvable through photometric variations. However, even when the SNR for photometric variability is high enough to be resolved, false positives may come from several other sources of uncertainties (Brown 2003; Sullivan et al. 2015; Kane et al. 2016; Simpson et al. 2022). To minimize the possibility of false positives, we impose an additional condition, $M_{\text{BH}} \geq M_{\text{LC}}$. We call the subset of BH–LC binaries satisfying this additional condition as the ‘pessimistic’ set. This additional condition $M_{\text{BH}} \geq M_{\text{LC}}$ ensures that a potential candidate LC exhibiting the desired photometric variation not only is the dominant source of light, but also is lower mass compared to the dark companion. Note however, even this additional condition may not be enough to rule out all possibilities of impostor BHs, especially in case of post main sequence (PMS) companions. A prominent example

would be algol-type binaries where PMS components are paired with more massive non-degenerate companions (Gomel, R. et al. 2023). Hence, photometric variations alone are likely not adequate for confirmation of BH–LC binaries. These should be considered as candidates ripe for followup spectroscopic observations.

4. RESULTS

In this section, we describe the key properties of the present-day simulated BH–LC populations and discuss the detectable populations from EV, RB or SL. We have already discussed the intrinsic populations without any restrictions in Paper I. We encourage readers to refer to Paper I for an exhaustive discussion on the present-day intrinsic BH–LC properties in the MW. Here we highlight a few key properties for which binary interactions and the choice of supernova physics leave clear imprints directly influencing their detectability via photometric variations. A view to the intrinsic properties also helps illuminate the effects of selection biases in identifying the detectable populations. Throughout this work we focus only on detached BH–LC binaries with $P_{\text{orb}}/\text{yr} \leq 3$ and $P_{\text{orb}}/\text{yr} \leq 10$ keeping in mind the maximum observation durations of TESS and *Gaia*. The sizes of the TESS and *Gaia*-detectable BH–LC populations for each set of binary models and observational selection cuts are summarized in Table 1 and 2.

4.1. Intrinsic BH–LC population

Figure 1 shows the distributions of M_{BH} , E_{cc} , and M_{LC} of the present day detached BH–LC populations for the **rapid** and **delayed** models with the relevant upper limits on P_{orb} . The characteristics of the intrinsic present-day populations depend strongly on the SNe explosion mechanism and the adopted binary evolution model which encodes mass transfer physics, stellar winds, and tidal evolution. However, we do not find significant differences between these distributions corresponding to $P_{\text{orb}}/\text{yr} \leq 3$ and $P_{\text{orb}}/\text{yr} \leq 10$. The M_{BH} distribution spans the complete allowed $3 - 45 M_{\odot}$ for both **rapid** and **delayed** models, however, striking difference is apparent near the so-called ‘lower mass-gap’ between $3 - 5 M_{\odot}$. While, both core-collapse SNe and AIC contribute in populating the BHs with $3 \leq M_{\text{BH}}/M_{\odot} \leq 5$ in the **delayed** model, the BHs in this mass range in the **rapid** model are produced from AIC only (Fryer et al. 2012). As a result, the **rapid** (**delayed**) model consists $\sim 1\%$ ($\sim 55\%$) of BH–LC

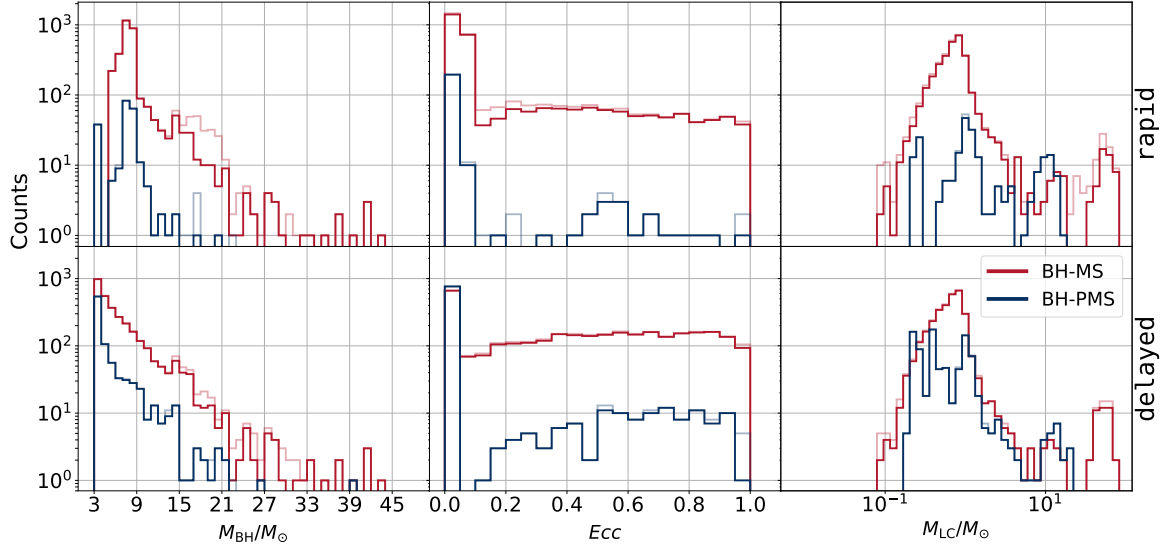


Figure 1. M_{BH} , Ecc and M_{LC} distributions of the present-day detached BH-LC binaries in the MW from our **rapid**(top) and **delayed**(bottom) models. The bright and faded curves represent detached BH-LCs with $P_{\text{orb}}/\text{yr} \leq 3$ and 10, respectively. The red and blue curves represent BH-MS and BH-PMS, respectively. The distributions from the **rapid** and **delayed** models show significant differences between $M_{\text{BH}}/M_{\odot} = 3$ –5. BHs in this range come only from AIC of NSs in the **rapid** model, whereas, the **delayed** model allows BH formation both via AIC and CCSNe in this range.

Table 1. BH-LC detectable population in the Milky Way by *Gaia*

Model	Type	Optimistic			Pessimistic($M_{\text{BH}} \geq M_{\text{LC}}$)		
		EV	RB	SL	EV	RB	SL
rapid	MS	358^{+24}_{-23} (765 $^{+34}_{-29}$)	772^{+42}_{-37} (1, 193 $^{+48}_{-43}$)	77^{+13}_{-11} (77 $^{+13}_{-11}$)	333^{+25}_{-21} (678 $^{+34}_{-28}$)	510^{+30}_{-28} (920 $^{+37}_{-36}$)	63^{+11}_{-9} (63 $^{+11}_{-9}$)
	PMS	193^{+17}_{-21} (256 $^{+18}_{-20}$)	173^{+16}_{-17} (305 $^{+20}_{-22}$)	24^{+5}_{-6} (24 $^{+5}_{-6}$)	160^{+16}_{-17} (211 $^{+16}_{-17}$)	116^{+11}_{-14} (238 $^{+17}_{-18}$)	24^{+5}_{-6} (24 $^{+5}_{-6}$)
	total	550^{+29}_{-29} (1, 024 $^{+38}_{-34}$)	942^{+46}_{-33} (1, 501 $^{+46}_{-50}$)	102^{+13}_{-13} (102 $^{+13}_{-13}$)	493^{+25}_{-25} (889 $^{+35}_{-31}$)	624^{+31}_{-28} (1, 159 $^{+38}_{-38}$)	86^{+13}_{-10} (86 $^{+13}_{-10}$)
delayed	MS	299^{+17}_{-24} (544 $^{+29}_{-26}$)	355^{+26}_{-24} (659 $^{+33}_{-30}$)	58^{+8}_{-8} (58 $^{+8}_{-8}$)	252^{+18}_{-19} (459 $^{+27}_{-26}$)	237^{+20}_{-18} (538 $^{+33}_{-28}$)	44^{+7}_{-8} (44 $^{+7}_{-8}$)
	PMS	131^{+13}_{-14} (163 $^{+14}_{-17}$)	62^{+9}_{-12} (189 $^{+19}_{-17}$)	18^{+7}_{-5} (18 $^{+7}_{-5}$)	127^{+13}_{-14} (157 $^{+12}_{-17}$)	56^{+9}_{-9} (181 $^{+16}_{-18}$)	18^{+7}_{-5} (18 $^{+7}_{-5}$)
	total	428^{+28}_{-28} (707 $^{+35}_{-33}$)	418^{+27}_{-26} (850 $^{+38}_{-37}$)	76^{+11}_{-11} (76 $^{+11}_{-11}$)	379^{+23}_{-27} (615 $^{+32}_{-32}$)	294^{+23}_{-22} (719 $^{+35}_{-36}$)	62^{+10}_{-10} (62 $^{+10}_{-10}$)

NOTE—Expected number of detached BH-LC binaries detectable by *Gaia* from EV, RB and SL with $\text{SNR} \geq 10$ (1) in the present-day Milky Way. The numbers and errors denote the median and the spread between the 10th and 90th percentiles across the Milky-Way realisations.

binaries with $M_{\text{BH}}/M_{\odot} \leq 5$. Of the BH-LCs in the **delayed** model with M_{BH} in the lower mass-gap, $\sim 10\%$ are produced from AIC and the rest are from CCSNe.

The Ecc distribution of the present-day population of BH-LC binaries transforms from the initially-assumed thermal distribution through binary stellar evolution including tides, mass loss, mass transfer, and natal kicks during BH formation. The **rapid** and **delayed** SNe prescriptions, through differences in the wind mass loss, birth mass function of BHs, and the details of the explosion mechanism, produce differences in the Ecc distributions of present-day BH-LC binaries. We find that about 70% of BH-LCs have near-circular ($Ecc \leq 0.1$)

orbits in the **rapid** model, in contrast to only 40% of such systems in the **delayed** model.

We find wide spreads in M_{LC} . For example, for most BHs with post main-sequence (PMS) or MS companions in detached orbits with $P_{\text{orb}} \leq 3\text{yr}$, $0.1 \lesssim M_{\text{LC}}/M_{\odot} \lesssim 20$. We find no significant difference between the M_{LC} distributions for BH binaries with $P_{\text{orb}}/\text{yr} \leq 3$ and ≤ 10 . While we do find detached BH-PMS binaries with $20 \lesssim M_{\text{LC}}/M_{\odot} \lesssim 35$, they have $P_{\text{orb}}/\text{yr} \geq 10$. Similarly, the majority of all BH-MS binaries with $M_{\text{LC}}/M_{\odot} \gtrsim 18$ have $P_{\text{orb}}/\text{yr} \geq 10$. Nevertheless, M_{LC} in detached BH-MS binaries with short $P_{\text{orb}}/\text{yr} \leq 3$ exhibit a larger spread compared to that in BH-PMS binaries. About

Table 2. BH–LC detectable population in the Milky Way by TESS

Model	Type	Optimistic			Pessimistic($M_{\text{BH}} \geq M_{\text{LC}}$)		
		EV	RB	SL	EV	RB	SL
rapid	MS	46^{+10}_{-8} (176 $^{+16}_{-16}$)	107^{+16}_{-12} (227 $^{+19}_{-22}$)	1 (3 $^{+3}_{-2}$)	19^{+6}_{-5} (116 $^{+13}_{-12}$)	34^{+8}_{-7} (149 $^{+15}_{-16}$)	1 (1 $^{+2}_{-1}$)
	PMS	38^{+9}_{-6} (78 $^{+13}_{-9}$)	58^{+12}_{-9} (105 $^{+13}_{-11}$)	0 (1 $^{+2}_{-1}$)	31^{+8}_{-6} (58 $^{+10}_{-9}$)	18^{+6}_{-5} (47 $^{+8}_{-9}$)	0 (1 $^{+1}_{-1}$)
	total	86^{+12}_{-10} (253 $^{+22}_{-18}$)	165^{+20}_{-16} (334 $^{+22}_{-23}$)	1 (4 $^{+3}_{-2}$)	51^{+10}_{-9} (175 $^{+17}_{-16}$)	52^{+10}_{-8} (196 $^{+14}_{-18}$)	0 (2 $^{+3}_{-1}$)
delayed	MS	42^{+10}_{-8} (117 $^{+14}_{-16}$)	44^{+10}_{-7} (118 $^{+15}_{-14}$)	0 (0)	17^{+6}_{-6} (75 $^{+13}_{-10}$)	7^{+4}_{-3} (75 $^{+12}_{-12}$)	0 (0)
	PMS	34^{+8}_{-7} (67 $^{+10}_{-11}$)	12^{+6}_{-4} (41 $^{+9}_{-9}$)	0 (0)	32^{+8}_{-7} (62 $^{+10}_{-9}$)	6^{+4}_{-2} (34 $^{+8}_{-8}$)	0 (0)
	total	77^{+13}_{-11} (183 $^{+22}_{-17}$)	57^{+10}_{-9} (159 $^{+17}_{-16}$)	0 (0)	48^{+10}_{-9} (136 $^{+17}_{-13}$)	14^{+5}_{-5} (109 $^{+14}_{-13}$)	0 (0)

NOTE—Same as Table 1 but for TESS detectable BH–LC population.

2.1% (1.4%) of the present-day BH–LC population contains MS companions with $M_{\text{LC}}/M_{\odot} \geq 35$ in the **rapid** (**delayed**) model. These are young binaries with ages ≤ 10 Myr and are created from initially short-period ($P_{\text{orb}}/\text{yr} \leq 5$) binaries where the LC’s progenitor got rejuvenated via mass accretion from the BH’s progenitor via Roche-love overflow (RLOF; Tout et al. 1997). Although only a small fraction of the overall population, these are potentially interesting systems. Over time, the high-mass LCs may evolve and create CO–CO binaries and be detected as a variety of interesting sources en-route. For example, during the later stage of the LC’s evolution, the BH may start accreting via RLOF and become detectable via X-ray or radio emissions. Furthermore, if the mass transfer process is unstable, CE evolution may initiate and make the final CO–CO binary compact enough to emit detectable GWs or merge. Although interesting, following the final fate of these binaries is beyond the scope of this study.

4.2. Gaia and TESS Detections

Table 1, 2 summarises the expected number of detections by *Gaia* and TESS via EV, RB, and SL with $\text{SNR} \geq 10$ (1). In addition, we list the expected numbers where $M_{\text{BH}} \geq M_{\text{LC}}$. For both *Gaia* and TESS, photometric variations from EV and RB are significantly easier to detect compared to SL which leads to roughly an order of magnitude fewer detectable sources. This is expected for several reasons. In general, the geometric probability for SL is low, especially because here we consider only detached binaries which requires higher P_{orb} . Even when the orientation allows SL, the magnification is typically low. Even if the maximum SL signal $\mu_{\text{SL,max}} = [1 + 4/(R_{\text{LC}}/R_{\text{E}})^2]^{1/2}$ is greater than the photometric precision, the large impact parameter (300–600 R_{E}) and short transit duration (~ 1 hr) makes detection challenging with the cadence we have considered for *Gaia* and TESS. The overall low yield from SL is

consistent with past studies (Rahvar et al. 2010; Masuda & Hotokezaka 2019; Wiktorowicz et al. 2021).

Of course, in reality, an acceptable SNR is often dependent on the environment and the source itself. Hence, it is always instructive to investigate how the detectable numbers vary as a function of SNR. Figure 2 shows the reverse cumulative distribution of detached BH–LC binaries detectable via the various channels of photometric variations. For **rapid**, in case of *Gaia*, the total number of detections using the optimistic cut with $\text{SNR} \geq 10$ (1) is 1074 (1502). The corresponding number using the pessimistic cut is 751 (1162). Similarly, for TESS, the expected numbers of detections with $\text{SNR} \geq 10$ and 1 for the optimistic (pessimistic) cut are 194 and 387 (80 and 250).

Contribution from EV and RB are typically close to each other for both *Gaia* and TESS. Detected systems with EV and RB also have a high overlap (Figure 3); detectable detached BH–LC binaries with EV and RB have an overlap of roughly 50% (67%) for TESS (*Gaia*). In both *Gaia* and TESS, almost all detectable systems via SL can also be detected via either RB or EV or both. Overall, the expected number of detections in the **rapid** model is higher by a factor of ≈ 2 compared to the **delayed** model. This is simply because the **rapid** model contains a higher proportion of higher-mass BHs compared to the **delayed** model (e.g., Fryer et al. 2012).

Note that, in our models, we adopt a very conservative lowest mass ($M_{\text{BH}}/M_{\odot} > 3$) for BHs. Thus, these simulated numbers are for expected detectable BH–LC binaries with at least $M_{\text{BH}}/M_{\odot} > 3$. This should reduce the possibility that the unseen object is a white dwarf or NS (Fonseca et al. 2021; Romani et al. 2022). Moreover, our additional condition used in the pessimistic cut, $M_{\text{BH}}/M_{\text{LC}} \geq 1$, should reduce false positives even further. Nevertheless, the confidence in identifying the nature of the dark component ultimately would depend

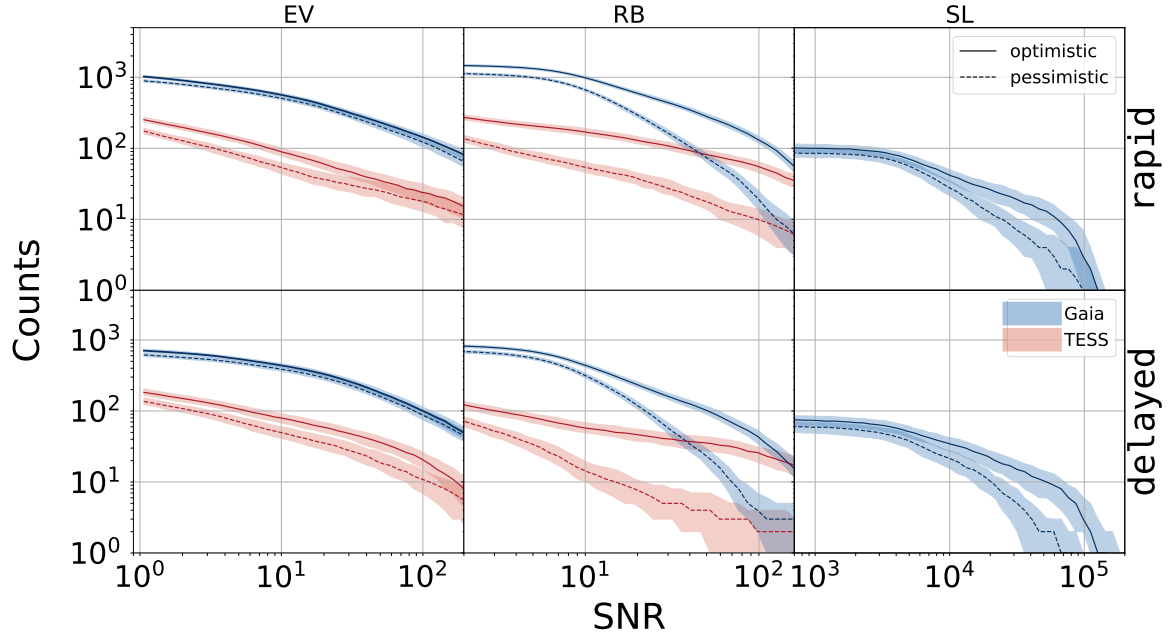


Figure 2. The reverse cumulative distribution of the expected detections of BH-LC binaries by EV (left) RB (middle) and SL (right) using TESS (red) and *Gaia* (blue) as a function of SNR for the **rapid** (top) and **delayed** (bottom) models. Solid and dashed lines represent the median number of detectable BH-LC binaries adopting the optimistic and pessimistic cuts (subsection 3.2). The shaded regions represent the spread between the 10th and the 90th percentiles due to statistical fluctuations between our 200 independent MW realisations.

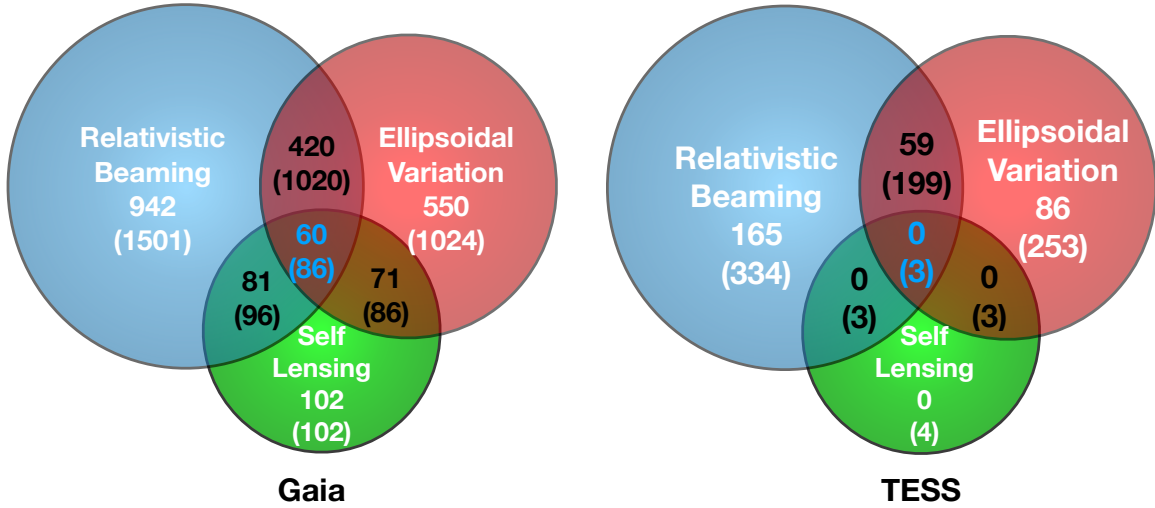


Figure 3. Number of BH-LC binaries resolvable via photometric variability by *Gaia* (left) and TESS (right) for the **rapid** model with $\text{SNR} \geq 10$ (1). Blue, red, and green denote populations resolvable via RB, EV, and SL signals, respectively. Numbers written in white, black, and blue denote total numbers for each set, number of systems with two and all three resolvable signals, respectively. For both telescopes, there are large ($\sim 50\%$) overlaps between populations resolvable via EV and RB. The relatively small fraction of BH-LCs with detectable SL would also be detectable either via RB or EV or both. (The equivalent figure (Figure A1) for our **delayed** model is presented in the Appendix.)

on the estimated errors in the mass and followup observations (e.g., Ganguly et al. 2023; Chakrabarti et al. 2023; El-Badry et al. 2022e; Shahaf et al. 2023). We envisage that while photometric variability can identify the interesting targets, multi-wavelength followup observations and RV followup will help to clearly identify the nature of the dark component in these binaries.

Interestingly, similar to the case of astrometrically detectable BH-LC binaries presented in Paper I, we find that the photometrically detectable BH-LC binaries also show little dependence on the BH mass (Figure 4, A2). This can be somewhat counter-intuitive since the strength of the signal increases with increasing M_{BH} for all physical effects we have considered here (see section 3). This is because, the detectability more strongly depends on the photometric precision of *Gaia* and TESS compared to the signal strength. The photometric precision, on the other hand, depends strongly on the magnitude of the LC (Rimoldini, Lorenzo et al. 2023) and does not depend at all on M_{BH} . As a result, the M_{BH} distribution of the detectable population is expected to closely resemble the intrinsic one. This is in contrast to BH populations detected from other more traditional observations like X-ray, radio, and GWs (Jonker et al. 2021; Liotine et al. 2023).

4.3. Key properties of the BH-LCs detectable via photometric variations

Overall, the distributions of key observable properties for the detectable population are very similar to those of the intrinsic population. Moreover, the TESS and *Gaia*-detectable populations are very similar in properties. Detectable differences in the population properties come from the differences in the adopted supernova prescription. We use $\text{SNR} \geq 10$ as the cutoff to determine the detectability, unless otherwise specified.

The distributions of the detected population through photometric variability show a wide spread in both Z and M_{BH} for both the **rapid** and **delayed** models (Figure 5). The M_{BH} distribution shows distinct features for the **rapid** and **delayed** models. The lower mass gap ($3-5 M_{\odot}$) in the intrinsic population for the **rapid** model remains apparent also in the detectable population; $\sim 6\%$ ($\sim 3\%$) of the TESS (*Gaia*) detectable BH-LC binaries contain BHs with $3 \leq M_{\text{BH}}/M_{\odot} \leq 5$ in the **rapid** model, in contrast to $\sim 75\%$ ($\sim 58\%$) in the **delayed** model. Of course, in the **rapid** model all detectable BHs in the mass gap must come from AIC of NSs. In contrast, in the **delayed** model, most ($\sim 78-92\%$) detectable BHs in this mass range come from CCSNe and the rest from AIC. Contribution from AIC is a little

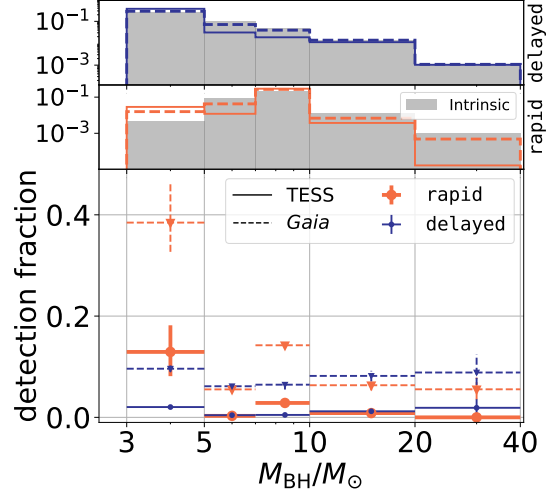


Figure 4. The ratio between the detectable binaries and intrinsic population (detection fraction) as a function of M_{BH} for the BH-LCs detectable via photometric variations using TESS (solid) and *Gaia* (dashed) for the **rapid** (orange) and **delayed** (blue) models. The vertical and horizontal error bars represent the 10–90th percentiles and the bin size in M_{BH} , respectively. The detection fraction is not strongly dependent on M_{BH} for photometrically detectable BH-LC populations from both SNe models. The gray histogram in the top panel represents the intrinsic M_{BH} distribution. Figure A2 illustrates varying the SNR threshold does not significantly affect the overlap between the intrinsic and observed populations.

higher (22% and 8% for TESS and *Gaia*) in the **delayed** model for detectable BHs with PMS companions.

The metallicities of the detectable detached BH-LCs show a wide spread, $-2.4 \leq \log(Z/Z_{\odot}) \leq 0.2$, although, the majority of the detectable population consist of young BH-LC’s with $Z \geq 0.02$. As a result, we find $M_{\text{BH}}/M_{\odot} \leq 20$ in the detectable population. The wide spread in metallicities is particularly interesting. Using astrometric and photometric observations it may be possible to put constraints on the LC properties including metallicity and age. Based on these constraints, it may be possible to constrain the age and metallicity of the BH’s progenitor in real systems. Furthermore, if the mass of the BHs can also be determined via photometric variations, astrometric solutions, or follow-up observations, then a metallicity-dependent map connecting BHs with their progenitors may emerge for a wide range in the observed metallicities.

A metallicity-dependent map between progenitor properties and the BHs they create can be instrumental in improving our understanding of high-mass stellar evolution and binary interaction. These BH-LC systems descend from massive ($M > 10 M_{\odot}$) stars and go through several metallicity-dependent, important, but

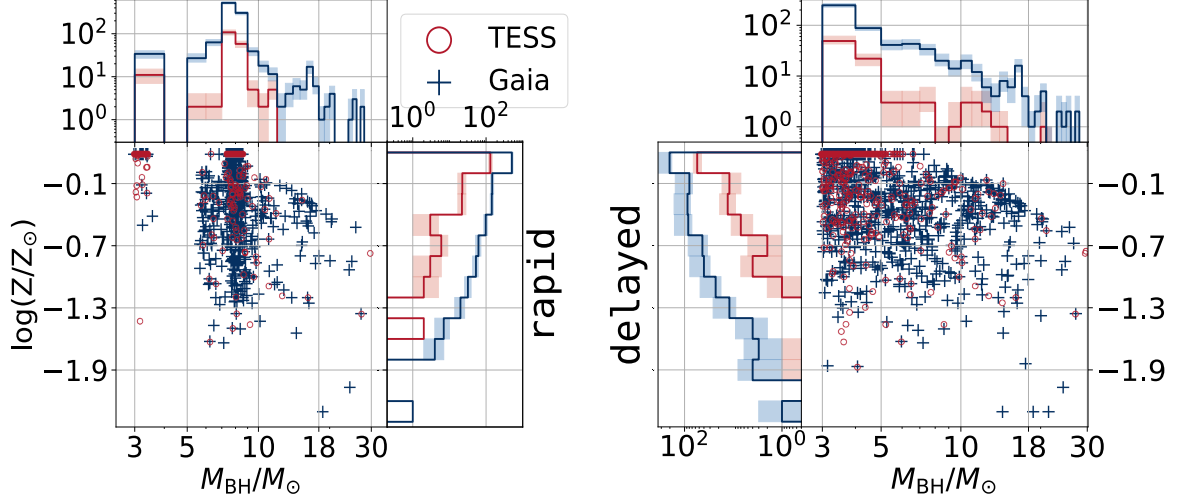


Figure 5. Distributions of M_{BH} and progenitor metallicity of the detached BH–LC binaries detectable through photometric variability. Red circle and blue plus represent populations detectable using TESS and *Gaia*, respectively. Lines and shades in the histograms represent median and the spread between the 10th and 90th percentiles in each bin. Left and right figures denote the **rapid** and **delayed** models.

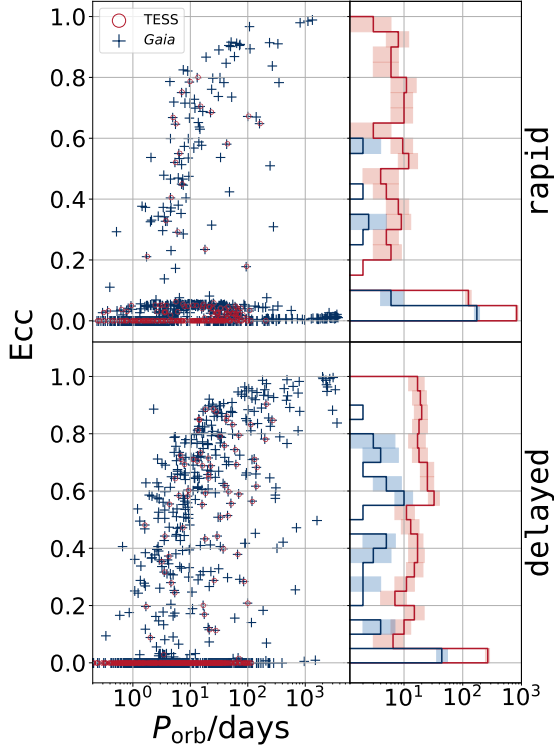


Figure 6. P_{orb} vs E_{cc} for BH–LCs detectable via photometric variations using TESS (red circle) and *Gaia* (blue plus) for our **rapid** (top) and **delayed** (bottom) models.

uncertain stages of evolution, such as mass-loss through winds, RLOF, and CE evolution. Thus, if indeed discovered in large numbers spanning a wide range in metallicities, the inferred mass of each component in the binary, combined with the metallicity and age of the LC, would help constrain models of the BH progenitor’s evolution

as well as high-mass binary stellar evolution via comparison between model and observed present-day properties of detached BH–LC binaries.

Apart from the M_{BH} distribution, the orbital eccentricities can also differentiate between different SN explosion mechanisms (also see Paper I). Majority ($\sim 60 - 98\%$) of the photometrically detectable BH–LCs in all our models go through at least one mass transfer or CE episode, which erases the initial orbital eccentricity. Thus, the final orbital eccentricity is almost entirely dependent on the natal kicks the BHs receive, which later can be further modified by tides depending on P_{orb} and the time since BH formation. Under the fallback-modulated prescription for natal kicks, the BHs in the **delayed** model typically receive larger kicks compared to those in the **rapid** model. As a result, the detectable BH–LC binaries in the **delayed** model contain a much larger fraction ($\sim 54\%$) of $E_{\text{cc}} > 0.1$ orbits compared to those in the **rapid** model ($6 - 11\%$). Figure 6 shows P_{orb} vs E_{cc} for the detectable populations. The **rapid** (**delayed**) model contains about 94% (46%) and 89% (47%) BH–LC binaries with $E_{\text{cc}} \leq 0.1$ in the TESS and *Gaia* detected populations. Because of the relatively stronger natal kicks the BHs receive, the **delayed** model contains a much higher fraction ($\sim 30 - 35\%$) of BH–LC binaries with $E_{\text{cc}} > 0.5$ compared to the **rapid** model ($3 - 8\%$) in the TESS as well as *Gaia* detected populations. These observable differences in the E_{cc} distributions can be really interesting if detached BH–LCs are indeed discovered in large numbers through photometric as well as astrometric channels. Since, the final orbital E_{cc} is essentially dependent on natal kicks, a careful study of the E_{cc} distribution for these systems

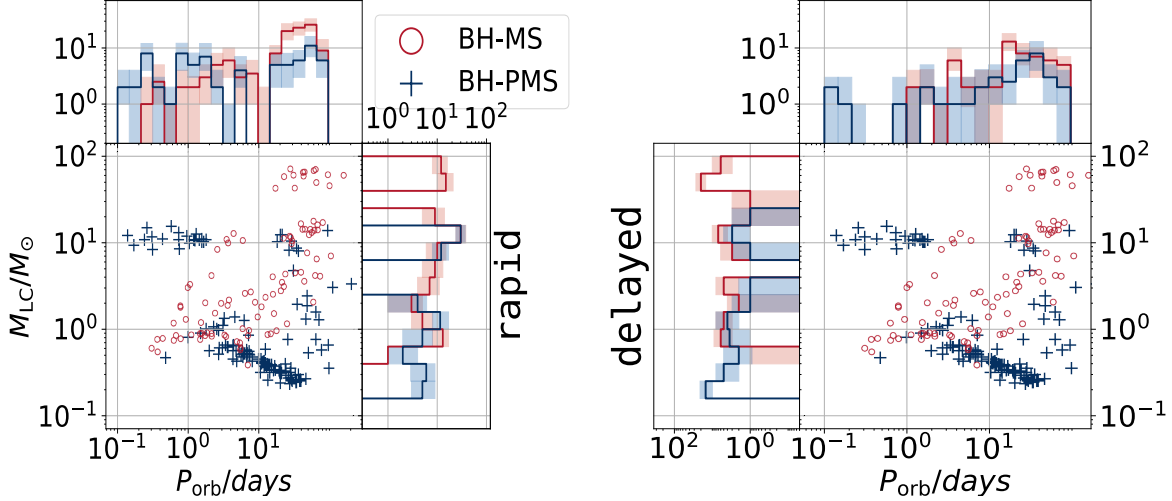


Figure 7. Distribution of P_{orb} vs M_{LC} for detached BH-LCs detectable via photometric variability using TESS. Red circles and blue crosses represent BH-MS and BH-PMS binaries, respectively. Note the correlation between P_{orb} and M_{LC} , especially for the detectable BH-MS binaries.

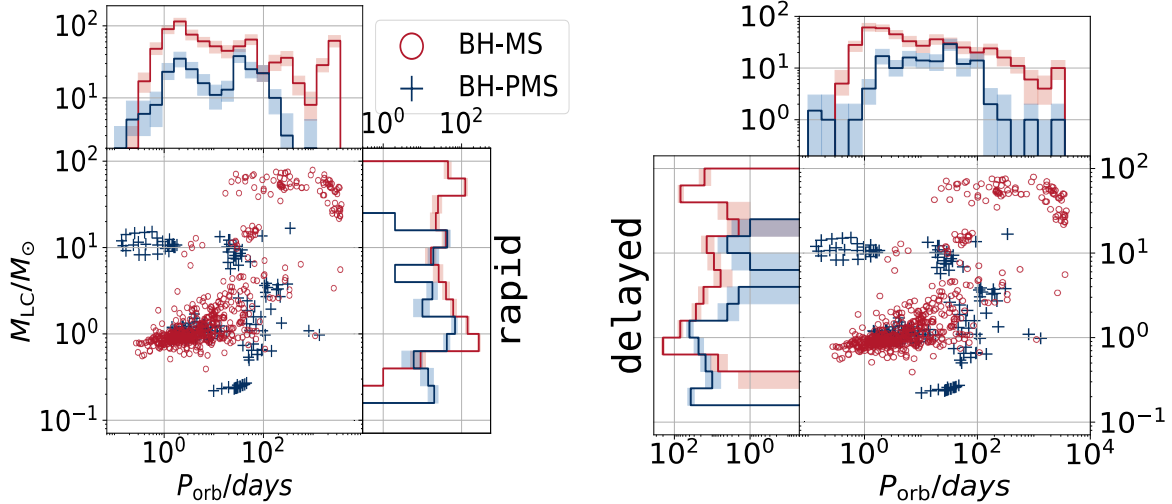


Figure 8. Same as Figure 7 but for BH-LCs detectable through photometric variability using *Gaia*.

should help in constraining poorly understood natal kick physics (Repetto et al. 2017; Atri et al. 2019; Andrews & Kalogera 2022; Shikauchi et al. 2023).

We find that the P_{orb} distributions for the detectable BH-LCs exhibit diverse ranges extending up to ~ 100 days for TESS and ~ 10 years for *Gaia*, essentially limited by the observation duration (Figure 7, 8), which also indicates that almost all detectable binaries have been observed for multiple transits. At first glance this is counter-intuitive because the signal is expected to be stronger for shorter P_{orb} for all channels of photometric variability (Equation 4, 6). This can be understood as a consequence of subtle effects from the formation channel of the BH-LC binaries detectable through photometric variations. Most ($\approx 45 - 71\%$ for TESS and $80 - 84\%$ for *Gaia*) detectable BH-LCs have gone through at least

one CE episode during their evolution. The eventual detached configuration, for the majority of the detectable BH-LCs thus depends on when the CE ends. All else kept fixed, a lower-mass LC would require a larger orbital decay before the CE can be ejected. This introduces a correlation between P_{orb} and M_{LC} (Figure 7, 8). A higher M_{LC} means a brighter target, which in turn means lower photometric noise, all else kept fixed. Thus, a combination of population properties as well as selection biases effectively reduces the strong P_{orb} dependence of the signal strength in the detectable population.

Overall, we find that CE evolution plays a major role in shaping the properties of the BH-LCs detectable through photometric variability. For BH-MS binaries in the **rapid** and **delayed** models, 77% and 52% (75%

and 80%) of the TESS (*Gaia*) detectable populations go through at least one CE evolution. In case of BH–PMS binaries, between 10 to 20% of the detectable systems go through CE evolution more than once. The detectable BH–PMS binaries also show interesting clustering in the P_{orb} vs M_{LC} plane. The short- P_{orb} group contains systems with significantly higher M_{LC} compared to that with longer P_{orb} . The more compact BH–PMS binaries initially had massive progenitors ($M_{\text{LC,ZAMS}} \geq 20 M_{\odot}$) in tight orbits ($P_{\text{orb}} \lesssim 10^2$ days). For these binaries, the CE is initiated by mass transfer from the LC and at the time of observation, the LC is a stripped Helium star. These are all younger than 8 Myr at the time of observation. Because of the prevalence of CE evolution in the detectable BH–LCs, the properties of the observed populations may be able to put meaningful constraints on the uncertain aspects of CE evolution (Ivanova et al. 2013; Hirai & Mandel 2022; Renzo et al. 2023).

5. COMBINATION OF DIFFERENT DETECTION CHANNELS

Discovery of a population of stellar BHs in detached orbits with a LC is almost certainly going to receive a huge boost by combining various methods and followup studies. Indeed, several studies have identified candidate BH–LC binaries via various methods and combinations of them using *Gaia*’s third data release (DR3; Andrews et al. 2022; Fu et al. 2022; Gomel, R. et al. 2023; Jayasinghe et al. 2023; Shahaf et al. 2022; El-Badry et al. 2022e). In Paper I, we highlighted that a large population of detached BH–LC binaries may be resolvable by *Gaia*’s astrometry and that astrometry alone is likely to put strong enough constraints on the dark object’s mass to clearly indicate a BH. Furthermore, we highlighted that *Gaia*’s RV with a spectral resolution of $R \sim 11,500$ for stars brighter than $G = 17$ (Cropper, M. et al. 2018; Soubiran, C. et al. 2018; Sartoretti, P. et al. 2023), itself could resolve the orbital motion for $\sim 50 - 120$ astrometrically resolvable binaries depending on the model assumptions. Of course, once the candidates are identified, spectroscopic followup using higher-precision instruments can significantly improve these yields, but since *Gaia*’s RV will automatically become available without any need for extensive followup, we only focus on that.

Based on *Gaia*’s pre-mission estimates, the radial-velocity measurements were expected to be available for sources brighter than $G = 17$ (Jordi et al. 2010). However, with the DR3 release, the multi-epoch RV measurements are only available for sources with $G \leq 14$. Considering both end of mission expectation and the, likely more realistic, threshold obtained from DR3, we

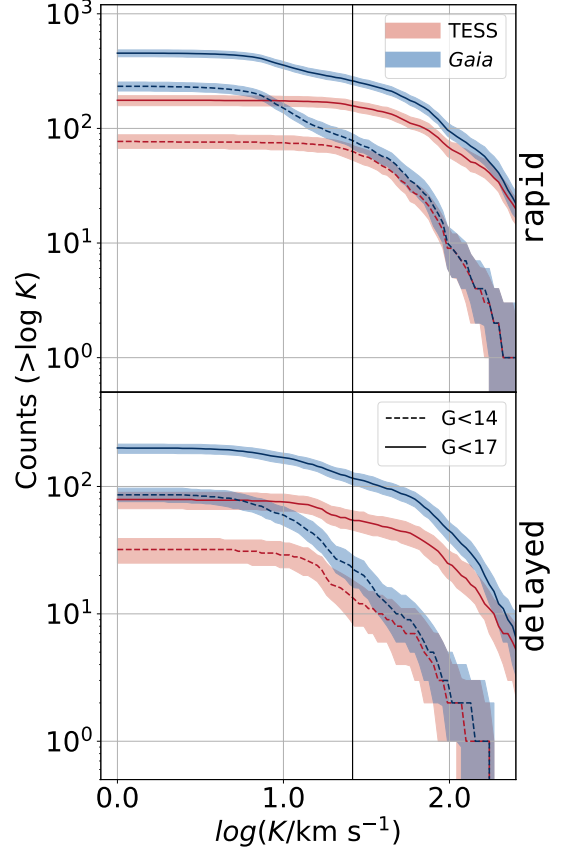


Figure 9. The reverse cumulative distribution of the RV semi-amplitude for detached BH–LCs resolvable via photometric variability using *Gaia* (blue) and TESS (red). The solid and dashed lines denote the BH–LC binaries with $G \leq 17$ and 14, respectively. Lines denote the median and the shaded regions denote the 10th and 90th percentiles from statistical fluctuations. Black vertical line denotes the minimum resolvable K by *Gaia*.

identify the photometrically resolvable ($\text{SNR} \geq 10$) BH–LC populations with $G \leq 14$ (17), which would also be resolvable by *Gaia*’s spectroscopy. Figure 9 shows the reverse cumulative distribution of the RV semi-amplitude for BH–LCs brighter than $G = 14$ (17) and resolvable through photometric variability by TESS and *Gaia*. The vertical line shows *Gaia*’s spectral resolution cutoff. We find that 62_{-9}^{+9} (158_{-17}^{+15}) and 14_{-10}^{+10} (55_{-10}^{+10}) BH–LCs for $G \leq 14$ (17) in the TESS resolved population would also be resolved with the help of spectroscopy in the **rapid** and **delayed** models, respectively. Similarly, the numbers for spectroscopically resolved BH–LC binaries in case of *Gaia* photometry are 78_{-11}^{+11} (260_{-19}^{+24}) and 23_{-6}^{+6} (116_{-12}^{+14}). Interestingly, 25%–60% of all photometrically detectable BH–LC binaries brighter than $G = 17$, (15–30% overall) are expected to have RV resolvable by *Gaia*. Thus, a combination of photometric detection and *Gaia*’s RV analysis is expected to provide credence

to these discoveries and allow better characterisation of orbital and stellar properties.

Figure 10 shows the detection fraction as function of P_{orb} for detached BH–LCs detected via TESS and *Gaia* photometry and *Gaia*’s astrometry. In case of *Gaia*’s astrometry, the detection fraction monotonically increases until it saturates for $P_{\text{orb}} \gtrsim 100$ days. This of course is easy to understand; the larger the orbit, the easier it is to resolve via astrometry. The trend for the photometrically resolvable populations is more nuanced. In this case, both for *Gaia* and TESS, the detection fraction first increases with increasing P_{orb} , peaks around $P_{\text{orb}}/\text{day} = 10\text{--}100$ ($P_{\text{orb}}/\text{day} = 100\text{--}1,000$) for TESS (*Gaia*) before decreasing. The peak is created due to the competition between two separate effects. The photometric variability signal depends strongly on P_{orb} , the more compact the orbit, the stronger the signal. As a result, for sufficiently large P_{orb} , the signal is simply too weak resulting in a decrease in the detection fraction. On the other hand, most detectable BH–LCs come from CE evolution. As a result, there is a distinct correlation between P_{orb} and M_{LC} (Figure 7, 8) and as a result, the magnitude. Hence, as P_{orb} increases, the photometric variability is easier to detect because of the lower noise for the brighter LCs. The different locations of the peaks for *Gaia* and TESS are reflective of their different observation duration.

Figure 11 shows the expected yields for detached BH–LCs from different detection channels and the overlap. We find between 10 – 30% (depending on the adopted SNe model) of the photometrically detectable BH–LCs would also be resolvable via astrometry. On the other hand, between 5–30% of the photometrically detectable BH–LCs are expected to have large enough RV to be resolved by *Gaia*’s spectroscopy. Overall, about 5–20% of all BH–LCs could be detectable from astrometry, photometry, as well as RV.

Once the BH–LC candidates are identified considering an appropriate cut-off SNR and other resolvability criteria, the characterization of the nature of the dark companion must be based on the M_{BH} estimate from follow-up RV and astrometric measurements. Note that, the RV followup need not be limited to *Gaia* only. Furthermore, even in the absence of follow-up observations, light curve fitting of the photometric signal can be used to constrain the minimum M_{BH} assuming edge-on orbit (Gomel et al. 2021; Rowan et al. 2021).

6. COMPARISON WITH *Gaia* OBSERVED EV CANDIDATES

Using *Gaia*’s third data release, Gomel, R. et al. (2023) constructed a catalog of 6000 detached CO–LC

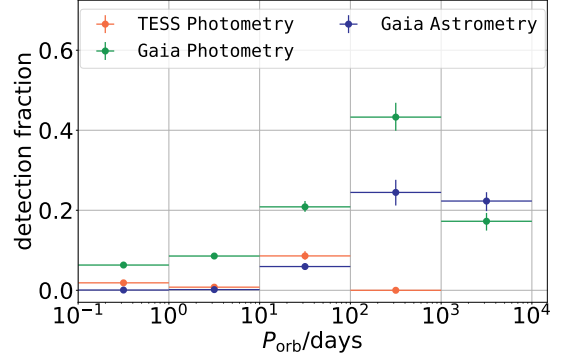


Figure 10. Detection fraction of detached BH–LC binaries as a function of P_{orb} via *Gaia*’s astrometry (blue), TESS photometry (orange), and *Gaia*’s photometry (green) for the **rapid** model. Dots and error bars represent median, 10th, and 90th percentiles in each bin. Detection fraction via astrometry increases with increasing P_{orb} until it saturates for $P_{\text{orb}}/\text{day} \gtrsim 10^2$. In contrast, detection fraction from photometry exhibits a peak. At large P_{orb} , the decrease from the peak detection fraction is due to reduced photometric variability signal, whereas, at the small P_{orb} , the decrease is due to the correlation between P_{orb} and M_{LC} in the BH–LC binaries (Figure 7,8). (The equivalent figure (Figure A3) for our **delayed** model is presented in the Appendix.)

candidate binaries identified using periodic flux variability. The study was predominantly focused on searching for CO–MS binaries in short-period ($P_{\text{orb}}/\text{day} \leq 2.5$) orbits. They avoided potential CO–PMS binaries because of a higher expected false-alarm rate (Gomel et al. 2021; Gomel, R. et al. 2023). These candidates have $13 \leq G \leq 20$. Their inferred modified minimum mass-ratio $q_{\text{min}} = M_{\text{CO}}/M_{\text{LC}}$, is the mass-ratio assuming an edge-on orientation and a fillout factor of 0.95 (Gomel et al. 2020). Their BH–LC candidates have $0.5 \leq q_{\text{min}} \leq 10$.

We perform mock observation of our model BH–MS binaries with $\text{SNR} > 10$. While for the SNR calculation, we generate orientations of our model BH–MS binaries, we assume edge-on configuration independent of these orientations, to calculate q_{min} for a direct comparison. Figure 12 shows P_{orb} vs q_{min} for candidate observed (Gomel, R. et al. 2023) and our model binaries. The model BH–LC binaries with $P_{\text{orb}}/\text{yr} \leq 10$ exhibit q_{min} between 0.01 and 40. We find a clear anti-correlation between q_{min} and P_{orb} stemming from the $P_{\text{orb}}\text{--}M_{\text{LC}}$ correlation in BH–MS binaries arising from CE evolution (subsection 4.3; Figure 7,8). Binaries with low q_{min} contain rejuvenated massive LCs, where the LC progenitor have previously accreted mass from the BH progenitor through stable RLOF. We also find in our simulated population that the P_{orb} distribution has a peak around 2.5 days for the BH–MS population and

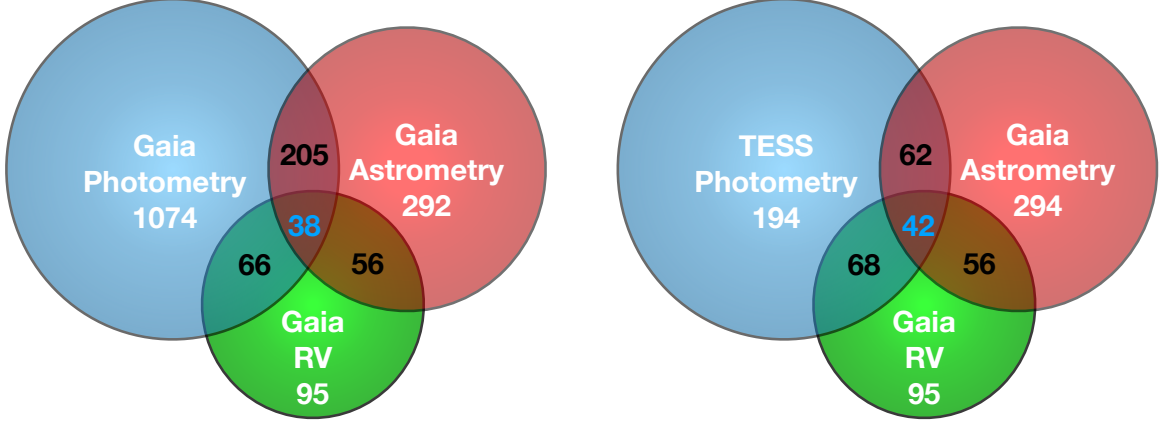


Figure 11. The expected numbers of detections from photometry (blue), *Gaia*'s astrometry (red), and *Gaia*'s RV (green) for detached BH-LC population for the **rapid** model and their overlap. The white, black, and blue numbers denote yields in each set, overlap between two, and three different channels, respectively. (The equivalent figure (Figure A4) for our **delayed** model is presented in the Appendix.)

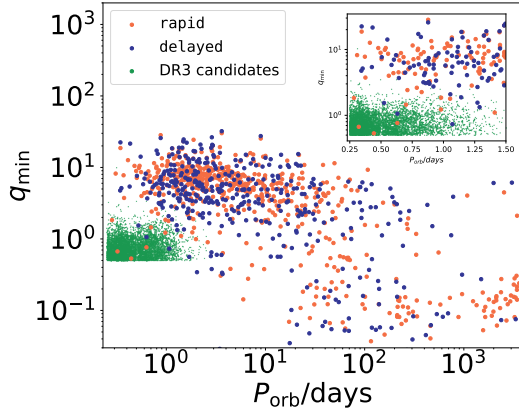


Figure 12. Mass ratio (q) vs P_{orb} distribution for *Gaia* detectable ($\text{SNR} \geq 10$) simulated BH-LC binaries and *Gaia* DR3 detached CO-LC candidates from Gomel, R. et al. (2023). Orange and blue dots represent simulated BH-LC binaries in the **rapid** and **delayed** model, while, green dots represent the *Gaia* observed CO-LC candidates.

a shifted peak 12 days for the BH-PMS population similar to that of Gomel et al. (2021). We find limited overlap between the observed candidates and our model binaries. This may be because most of the observed CO candidates may be WDs or NSs, and not BHs. On the other hand, in future if the number of photometrically detected BH candidates increases, and spans a wider range in P_{orb} , we predict an anticorrelation.

In Figure 13 we show our model detectable BH binaries (colored dots) with respect to *Gaia*'s color-magnitude diagram (CMD), the grey dots represent all *Gaia* sources. The simulated BH-LCs align well with the MS and PMS giant regions on the CMD. The simulated resolvable BH-MS binaries brighter and bluer than the MS turn-off depict the rejuvenated sources. Overall,

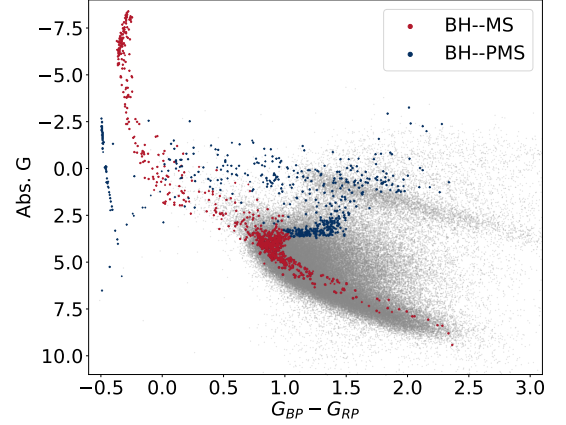


Figure 13. Distribution of BH-LC binaries in the *Gaia*'s color magnitude diagram. The grey dots in the background represents stellar sources from *Gaia* archive, the simulated BH-MS and BH-PMS binaries are represented by red and blue dots, respectively.

the CO-LC candidates identified from *Gaia*'s DR3 illustrate that a potential population of CO-LC candidates exist and more candidates are expected to be found in future data releases.

7. SUMMARY AND DISCUSSIONS

We have explored the possibility of detecting detached BH-LC binaries via photometric variability with TESS and *Gaia*. We create highly realistic present-day BH-LC populations using the BPS suite COSMIC (Breivik et al. 2020) taking into account a metallicity-dependent star formation history and the complex correlations between age, metallicity, and location of stars in the Milky Way (Wetzel et al. 2016; Hopkins et al. 2018; Sanderson et al. 2020). We have used two widely adopted SNe explosion mechanisms, rapid and delayed (Fryer et al. 2012), to

create two separate populations of present-day BH–LC binaries. We have shown the key observable features of the intrinsic BH–LC populations adopting appropriate P_{orb} limits (see subsection 4.1) as well as those that are expected to be detected via photometric variability (see subsection 4.2).

Using 200 realisations to take into account statistical fluctuations, taking into account different physical sources for photometric variability, TESS and *Gaia* selection biases, and three-dimensional extinction and reddening, we have generated a highly realistic population of detectable detached BH–LC binaries in the Milky Way at present (subsection 2.1, 3.2). In addition to detection through photometric variability, we have also analysed *Gaia*’s RV and astrometry to find relative yield and sources that could be detectable via multiple channels (see section 5).

- We predict about 50 – 200 and 300 – 1000 detached BH–LC binaries may be detected by TESS and *Gaia* through photometric variability arising primarily from EV and RB.
- The photometrically detectable BH–LCs are expected to have wide range in metallicity and host BHs spanning a wide range in mass (see Figure 5). This is potentially interesting since in such systems, if the LC properties such as age and metallicity can be observationally constrained, we may be able to find a direct connection between the BHs and their progenitor properties.
- The detection fraction is not strongly dependent on the BH mass (Figure 4). Thus, the detectable BHs are expected to be similar in properties to the intrinsic BHs in detached BH–LC binaries.
- The orbital Ecc is essentially determined by BH natal kicks. As a result, if detected in large numbers, the Ecc distribution can put constraints on natal kicks from core-collapse SNe.
- Since a majority ($\sim 45 - 84\%$) of BH–LCs detectable through photometric variability using TESS and *Gaia* go through at least one CE episode, there is an interesting correlation between P_{orb} and M_{LC} , especially for BH–MS binaries

(Figure 7, 8). It will be interesting to verify this trend. Moreover, since this stems primarily from the energetics of envelope ejection, if detected in large numbers as we predict, this population may put meaningful constraints on the various uncertain aspects of CE physics.

- A significant fraction of photometrically detectable BH–LC binaries may also be detectable via *Gaia*’s RV and astrometry (5–20% are detectable via all three methods, Figure 9, Figure 11), thus helping provide stronger constraints on their properties.

In Paper I, we showed the potential of *Gaia*’s astrometry for detecting and characterizing detached BH–LC binaries in large numbers. In this work we show that a combination of photometry, RV, and astrometry can significantly increase the number of identified detached BH–LC candidates. Especially, many detached BH–LCs are expected to be detectable via astrometry, RV, as well as photometry. Once identified, followup observations using more sophisticated instruments may improve the characterisation of these candidates even further. Our models suggest that we are on the verge of discovering a treasure trove in BH binaries, while the recent BH discoveries from *Gaia* astrometry (El-Badry et al. 2022e, 2023; Chakrabarti et al. 2023) whet our enthusiasm.

We thank the anonymous referee for insightful comments and constructive suggestions. CC acknowledges support from TIFR’s graduate fellowship. SC acknowledges support from the Department of Atomic Energy, Government of India, under project no. 12-R&D-TFR-5.02-0200 and RTI 4002. NS acknowledges TIFR’s visiting summer research program during which this project was initiated. All simulations were done using cloud computing on Azure. The Flatiron Institute is supported by the Simons Foundation.

Software: **Astropy** (Astropy Collaboration et al. 2013; Price-Whelan et al. 2018; Price-Whelan et al. 2022); **COSMIC** (Breivik et al. 2020); **mw dust** (Bovy et al. 2016); **isochrones** (Morton 2015); **matplotlib** (Hunter 2007); **numpy** (van der Walt et al. 2011); **scipy** (Virtanen et al. 2020); **ticgen** (Barclay 2017; Stassun et al. 2018); **tess-point** (Burke et al. 2020); **pandas** (Wes McKinney 2010); **sympy** (Meurer et al. 2017)

REFERENCES

- Abbott, B. P., Abbott, R., Abbott, T. D., et al. 2016a, Phys. Rev. Lett., 116, 1, doi: 10.1103/PhysRevLett.116.061102
- . 2016b, Phys. Rev. Lett., 116, 1, doi: 10.1103/PhysRevLett.116.241103

- . 2019, *Phys. Rev. X*, 9, 031040, doi: [10.1103/PhysRevX.9.031040](https://doi.org/10.1103/PhysRevX.9.031040)
- Abbott, R., Abbott, T. D., Abraham, S., et al. 2021a, *Physical Review X*, 11, 021053, doi: [10.1103/PhysRevX.11.021053](https://doi.org/10.1103/PhysRevX.11.021053)
- . 2021b, *ApJL*, 913, L7, doi: [10.3847/2041-8213/abe949](https://doi.org/10.3847/2041-8213/abe949)
- Abdurrahman, F. N., Stephens, H. F., & Lu, J. R. 2021, *The Astrophysical Journal*, 912, 146, doi: [10.3847/1538-4357/abee83](https://doi.org/10.3847/1538-4357/abee83)
- Alonso, R., Brown, T. M., Torres, G., et al. 2004, *The Astrophysical Journal*, 613, L153, doi: [10.1086/425256](https://doi.org/10.1086/425256)
- Ambartsumian, V. A. 1937, *AZh*, 14, 207
- Andrews, J. J., Breivik, K., & Chatterjee, S. 2019, *The Astrophysical Journal*, 886, 68, doi: [10.3847/1538-4357/ab441f](https://doi.org/10.3847/1538-4357/ab441f)
- Andrews, J. J., & Kalogera, V. 2022, *The Astrophysical Journal*, 930, 159, doi: [10.3847/1538-4357/ac66d6](https://doi.org/10.3847/1538-4357/ac66d6)
- Andrews, J. J., Taggart, K., & Foley, R. 2022, arXiv e-prints, arXiv:2207.00680, <https://arxiv.org/abs/2207.00680>
- Angus, R., Morton, T. D., Foreman-Mackey, D., et al. 2019, *The Astronomical Journal*, 158, 173, doi: [10.3847/1538-3881/ab3c53](https://doi.org/10.3847/1538-3881/ab3c53)
- Astropy Collaboration, Robitaille, T. P., Tollerud, E. J., et al. 2013, *A&A*, 558, A33, doi: [10.1051/0004-6361/201322068](https://doi.org/10.1051/0004-6361/201322068)
- Atri, P., Miller-Jones, J. C. A., Bahramian, A., et al. 2019, *Monthly Notices of the Royal Astronomical Society*, 489, 3116, doi: [10.1093/mnras/stz2335](https://doi.org/10.1093/mnras/stz2335)
- Auvergne, M., Bodin, P., Boissard, L., et al. 2009, *A&A*, 506, 411, doi: [10.1051/0004-6361/200810860](https://doi.org/10.1051/0004-6361/200810860)
- Bakos, G., Noyes, R. W., Kovács, G., et al. 2004, *Publications of the Astronomical Society of the Pacific*, 116, 266, doi: [10.1086/382735](https://doi.org/10.1086/382735)
- Barclay, T. 2017, *tessgi/ticgen: v1.0.0, v1.0.0*, Zenodo, doi: [10.5281/zenodo.888217](https://doi.org/10.5281/zenodo.888217)
- Barstow, M. A., Casewell, S. L., Catalan, S., et al. 2014, arXiv e-prints, arXiv:1407.6163, <https://arxiv.org/abs/1407.6163>
- Belczynski, K., Kalogera, V., Rasio, F. A., et al. 2008, *Astrophys. J. Suppl. Ser.*, 174, 223, doi: [10.1086/521026](https://doi.org/10.1086/521026)
- Bellinger, E. P., Hekker, S., Angelou, G. C., Stokholm, A., & Basu, S. 2019, *A&A*, 622, A130, doi: [10.1051/0004-6361/201834461](https://doi.org/10.1051/0004-6361/201834461)
- Bellm, E. C., Kulkarni, S. R., Graham, M. J., et al. 2018, *Publications of the Astronomical Society of the Pacific*, 131, 018002, doi: [10.1088/1538-3873/aaecbe](https://doi.org/10.1088/1538-3873/aaecbe)
- Bloemen, S., Marsh, T. R., Østensen, R. H., et al. 2011, *Monthly Notices of the Royal Astronomical Society*, 410, 1787, doi: [10.1111/j.1365-2966.2010.17559.x](https://doi.org/10.1111/j.1365-2966.2010.17559.x)
- Borucki, W. J., Koch, D. G., Basri, G., et al. 2011, *The Astrophysical Journal*, 736, 19, doi: [10.1088/0004-637x/736/1/19](https://doi.org/10.1088/0004-637x/736/1/19)
- Bovy, J., Rix, H.-W., Green, G. M., Schlafly, E. F., & Finkbeiner, D. P. 2016, *The Astrophysical Journal*, 818, 130, doi: [10.3847/0004-637x/818/2/130](https://doi.org/10.3847/0004-637x/818/2/130)
- Breivik, K., Chatterjee, S., & Andrews, J. J. 2019, *ApJL*, 878, L4, doi: [10.3847/2041-8213/ab21d3](https://doi.org/10.3847/2041-8213/ab21d3)
- Breivik, K., Chatterjee, S., & Larson, S. L. 2017, *The Astrophysical Journal*, 850, L13, doi: [10.3847/2041-8213/aa97d5](https://doi.org/10.3847/2041-8213/aa97d5)
- Breivik, K., Coughlin, S., Zevin, M., et al. 2020, *ApJ*, 898, 71, doi: [10.3847/1538-4357/ab9d85](https://doi.org/10.3847/1538-4357/ab9d85)
- Brown, G. E., & Bethe, H. A. 1994, *Astrophys. J.*, 423, doi: [10.1086/173844](https://doi.org/10.1086/173844)
- Brown, T. M. 2003, *The Astrophysical Journal*, 593, L125, doi: [10.1086/378310](https://doi.org/10.1086/378310)
- Burke, C. J., Levine, A., Fausnaugh, M., et al. 2020, *TESS-Point: High precision TESS pointing tool*, *Astrophysics Source Code Library*, <http://ascl.net/2003.001>
- Casares, J., Negueruela, I., Ribó, M., et al. 2014, *Nature*, 505, 378, doi: [10.1038/nature12916](https://doi.org/10.1038/nature12916)
- Chakrabarti, S., Simon, J. D., Craig, P. A., et al. 2023, *The Astronomical Journal*, 166, 6, doi: [10.3847/1538-3881/accf21](https://doi.org/10.3847/1538-3881/accf21)
- Chawla, C., Chatterjee, S., Breivik, K., et al. 2022, *The Astrophysical Journal*, 931, 107, doi: [10.3847/1538-4357/ac60a5](https://doi.org/10.3847/1538-4357/ac60a5)
- Claeys, J. S. W., Pols, O. R., Izzard, R. G., Vink, J., & Verbunt, F. W. M. 2014, *A&A*, 563, A83, doi: [10.1051/0004-6361/201322714](https://doi.org/10.1051/0004-6361/201322714)
- Cropper, M., Katz, D., Sartoretti, P., et al. 2018, *A&A*, 616, A5, doi: [10.1051/0004-6361/201832763](https://doi.org/10.1051/0004-6361/201832763)
- Drimmel, R., Cabrera-Lavers, A., & López-Corredoira, M. 2003, *Astron. Astrophys.*, 409, 205, doi: [10.1051/0004-6361:20031070](https://doi.org/10.1051/0004-6361:20031070)
- Duchêne, G., & Kraus, A. 2013, *Annual Review of Astronomy and Astrophysics*, 51, 269, doi: [10.1146/annurev-astro-081710-102602](https://doi.org/10.1146/annurev-astro-081710-102602)
- El-Badry, K., & Burdge, K. B. 2022, *Monthly Notices of the Royal Astronomical Society: Letters*, 511, 24, doi: [10.1093/mnras/lsab135](https://doi.org/10.1093/mnras/lsab135)
- El-Badry, K., Burdge, K. B., & Mróz, P. 2022a, *Monthly Notices of the Royal Astronomical Society*, 511, 3089, doi: [10.1093/mnras/stac274](https://doi.org/10.1093/mnras/stac274)
- El-Badry, K., & Quataert, E. 2021, *Monthly Notices of the Royal Astronomical Society*, 502, 3436, doi: [10.1093/mnras/stab285](https://doi.org/10.1093/mnras/stab285)

- El-Badry, K., Seeburger, R., Jayasinghe, T., et al. 2022b, *Monthly Notices of the Royal Astronomical Society*, 512, 5620, doi: [10.1093/mnras/stac815](https://doi.org/10.1093/mnras/stac815)
- El-Badry, K., Rix, H.-W., Quataert, E., et al. 2022e, *Monthly Notices of the Royal Astronomical Society*, 518, 1057, doi: [10.1093/mnras/stac3140](https://doi.org/10.1093/mnras/stac3140)
- El-Badry, K., Rix, H.-W., Cendes, Y., et al. 2023, *Monthly Notices of the Royal Astronomical Society*, 521, 4323, doi: [10.1093/mnras/stad799](https://doi.org/10.1093/mnras/stad799)
- Engel, M., Faigler, S., Shahaf, S., & Mazeh, T. 2020, *Monthly Notices of the Royal Astronomical Society*, 497, 4884, doi: [10.1093/mnras/staa2182](https://doi.org/10.1093/mnras/staa2182)
- Fonseca, E., Cromartie, H. T., Pennucci, T. T., et al. 2021, *The Astrophysical Journal Letters*, 915, L12, doi: [10.3847/2041-8213/ac03b8](https://doi.org/10.3847/2041-8213/ac03b8)
- Fryer, C. L., Belczynski, K., Wiktorowicz, G., et al. 2012, *Astrophys. J.*, 749, doi: [10.1088/0004-637X/749/1/91](https://doi.org/10.1088/0004-637X/749/1/91)
- Fryer, C. L., Olejak, A., & Belczynski, K. 2022, *ApJ*, 931, 94, doi: [10.3847/1538-4357/ac6ac9](https://doi.org/10.3847/1538-4357/ac6ac9)
- Fu, J.-B., Gu, W.-M., Zhang, Z.-X., et al. 2022, *The Astrophysical Journal*, 940, 126, doi: [10.3847/1538-4357/ac9b4c](https://doi.org/10.3847/1538-4357/ac9b4c)
- Fuchs, B., & Bastian, U. 2005, in *ESA Special Publication*, Vol. 576, *The Three-Dimensional Universe with Gaia*, ed. C. Turon, K. S. O’Flaherty, & M. A. C. Perryman, 573
- Gaia Collaboration, Arenou, F., Babusiaux, C., et al. 2023, *A&A*, 674, A34, doi: [10.1051/0004-6361/202243782](https://doi.org/10.1051/0004-6361/202243782)
- Ganguly, A., Nayak, P. K., & Chatterjee, S. 2023, *The Astrophysical Journal*, 954, 4, doi: [10.3847/1538-4357/ace42f](https://doi.org/10.3847/1538-4357/ace42f)
- Giesers, B., Dreizler, S., Husser, T. O., et al. 2018, *Mon. Not. R. Astron. Soc. Lett.*, 475, L15, doi: [10.1093/mnrasl/slx203](https://doi.org/10.1093/mnrasl/slx203)
- Giesers, B., Kamann, S., Dreizler, S., et al. 2019, *A&A*, 632, A3, doi: [10.1051/0004-6361/201936203](https://doi.org/10.1051/0004-6361/201936203)
- Goldberg, D., & Mazeh, T. 1994, *A&A*, 282, 801
- Gomel, R., Faigler, S., & Mazeh, T. 2020, *Monthly Notices of the Royal Astronomical Society*, 501, 2822, doi: [10.1093/mnras/staa3305](https://doi.org/10.1093/mnras/staa3305)
- . 2021, *Monthly Notices of the Royal Astronomical Society*, 504, 2115, doi: [10.1093/mnras/stab1047](https://doi.org/10.1093/mnras/stab1047)
- Gomel, R., Mazeh, T., Faigler, S., et al. 2023, *A&A*, 674, A19, doi: [10.1051/0004-6361/202243626](https://doi.org/10.1051/0004-6361/202243626)
- Gomez, S., & Grindlay, J. E. 2021, *The Astrophysical Journal*, 913, 48, doi: [10.3847/1538-4357/abf24c](https://doi.org/10.3847/1538-4357/abf24c)
- Gould, A. 1995, *ApJ*, 446, 541, doi: [10.1086/175812](https://doi.org/10.1086/175812)
- Gould, A., & Salim, S. 2002, *ApJ*, 572, 944, doi: [10.1086/340435](https://doi.org/10.1086/340435)
- Green, G. M., Schlafly, E., Zucker, C., Speagle, J. S., & Finkbeiner, D. 2019, *The Astrophysical Journal*, 887, 93, doi: [10.3847/1538-4357/ab5362](https://doi.org/10.3847/1538-4357/ab5362)
- Han, Z. 1998, *MNRAS*, 296, 1019, doi: [10.1046/j.1365-8711.1998.01475.x](https://doi.org/10.1046/j.1365-8711.1998.01475.x)
- Heggie, D. C. 1975, *Mon. Not. R. Astron. Soc.*, 173, doi: [10.1093/mnras/173.3.729](https://doi.org/10.1093/mnras/173.3.729)
- Herrero, E., Lanza, A. F., Ribas, I., et al. 2014, *A&A*, 563, A104, doi: [10.1051/0004-6361/201323087](https://doi.org/10.1051/0004-6361/201323087)
- Hirai, R., & Mandel, I. 2022, *The Astrophysical Journal Letters*, 937, L42, doi: [10.3847/2041-8213/ac9519](https://doi.org/10.3847/2041-8213/ac9519)
- Hobbs, G., Lorimer, D. R., Lyne, A. G., & Kramer, M. 2005, *Mon. Not. R. Astron. Soc.*, 360, doi: [10.1111/j.1365-2966.2005.09087.x](https://doi.org/10.1111/j.1365-2966.2005.09087.x)
- Hopkins, P. F., Wetzel, A., Kereš, D., et al. 2018, *MNRAS*, 480, 800, doi: [10.1093/mnras/sty1690](https://doi.org/10.1093/mnras/sty1690)
- Hu, Z.-C., Yang, Y.-L., Wen, Y.-H., Shen, R.-F., & Tam, P.-H. T. 2023, *Research in Astronomy and Astrophysics*, 23, 085008, doi: [10.1088/1674-4527/accc73](https://doi.org/10.1088/1674-4527/accc73)
- Hunter, J. D. 2007, *Computing in Science and Engineering*, 9, 90, doi: [10.1109/MCSE.2007.55](https://doi.org/10.1109/MCSE.2007.55)
- Hurley, J. R., Pols, O. R., & Tout, C. A. 2000, *MNRAS*, 315, 543, doi: [10.1046/j.1365-8711.2000.03426.x](https://doi.org/10.1046/j.1365-8711.2000.03426.x)
- Hurley, J. R., Tout, C. A., & Pols, O. R. 2002, *Mon. Not. R. Astron. Soc.*, 329, doi: [10.1046/j.1365-8711.2002.05038.x](https://doi.org/10.1046/j.1365-8711.2002.05038.x)
- Ivanova, N., Justham, S., Chen, X., et al. 2013, *A&A Rv*, 21, 59, doi: [10.1007/s00159-013-0059-2](https://doi.org/10.1007/s00159-013-0059-2)
- Ivezić, Ž., Kahn, S. M., Tyson, J. A., et al. 2019, *ApJ*, 873, 111, doi: [10.3847/1538-4357/ab042c](https://doi.org/10.3847/1538-4357/ab042c)
- Janssens, S., Shenar, T., Sana, H., et al. 2022, *A&A*, 658, A129, doi: [10.1051/0004-6361/202141866](https://doi.org/10.1051/0004-6361/202141866)
- Jayasinghe, T., Rowan, D. M., Thompson, T. A., Kochanek, C. S., & Stanek, K. Z. 2023, *Monthly Notices of the Royal Astronomical Society*, 521, 5927, doi: [10.1093/mnras/stad909](https://doi.org/10.1093/mnras/stad909)
- Jayasinghe, T., Stanek, K. Z., Thompson, T. A., et al. 2021, *MNRAS*, 504, 2577, doi: [10.1093/mnras/stab907](https://doi.org/10.1093/mnras/stab907)
- Jeans, J. H. 1919, *Monthly Notices of the Royal Astronomical Society*, 79, 408, doi: [10.1093/mnras/79.6.408](https://doi.org/10.1093/mnras/79.6.408)
- Jonker, P. G., Kaur, K., Stone, N., & Torres, M. A. P. 2021, *The Astrophysical Journal*, 921, 131, doi: [10.3847/1538-4357/ac2839](https://doi.org/10.3847/1538-4357/ac2839)
- Jordi, C., Gebran, M., Carrasco, J. M., et al. 2010, *Astron. Astrophys.*, 523, doi: [10.1051/0004-6361/201015441](https://doi.org/10.1051/0004-6361/201015441)
- Kane, S. R., Thirumalachari, B., Henry, G. W., et al. 2016, *The Astrophysical Journal*, 820, L5, doi: [10.3847/2041-8205/820/1/15](https://doi.org/10.3847/2041-8205/820/1/15)

- Khokhlov, S. A., Miroshnichenko, A. S., Zharikov, S. V., et al. 2018, *The Astrophysical Journal*, 856, 158, doi: [10.3847/1538-4357/aab49d](https://doi.org/10.3847/1538-4357/aab49d)
- Khruzina, T., Cherepaschuk, A., Shakura, N., & Sunyaev, R. 1988, *Advances in Space Research*, 8, 237, doi: [https://doi.org/10.1016/0273-1177\(88\)90413-9](https://doi.org/10.1016/0273-1177(88)90413-9)
- Kochanek, C. S., Shappee, B. J., Stanek, K. Z., et al. 2017, *Publications of the Astronomical Society of the Pacific*, 129, 104502, doi: [10.1088/1538-3873/aa80d9](https://doi.org/10.1088/1538-3873/aa80d9)
- Kollmeier, J. A., Zasowski, G., Rix, H.-W., et al. 2017, *arXiv e-prints*, arXiv:1711.03234, doi: [10.48550/arXiv.1711.03234](https://doi.org/10.48550/arXiv.1711.03234)
- Kopal, Z. 1959, *Close binary systems*
- Kroupa, P. 2001, *Mon. Not. R. Astron. Soc.*, 322, doi: [10.1046/j.1365-8711.2001.04022.x](https://doi.org/10.1046/j.1365-8711.2001.04022.x)
- Lam, C. Y., Lu, J. R., Udalski, A., et al. 2022, *The Astrophysical Journal Letters*, 933, L23, doi: [10.3847/2041-8213/ac7442](https://doi.org/10.3847/2041-8213/ac7442)
- Leibovitz, C., & Hube, D. P. 1971, *A&A*, 15, 251
- Lennon, D. J., Dufton, P. L., Villaseñor, J. I., et al. 2022, *A&A*, 665, A180, doi: [10.1051/0004-6361/202142413](https://doi.org/10.1051/0004-6361/202142413)
- Lin, J., Dotter, A., Ting, Y.-S., & Asplund, M. 2018, *Monthly Notices of the Royal Astronomical Society*, 477, 2966, doi: [10.1093/mnras/sty709](https://doi.org/10.1093/mnras/sty709)
- Liotine, C., Zevin, M., Berry, C. P. L., Doctor, Z., & Kalogera, V. 2023, *The Astrophysical Journal*, 946, 4, doi: [10.3847/1538-4357/acb8b2](https://doi.org/10.3847/1538-4357/acb8b2)
- Liu, J., Zhang, H., Howard, A. W., et al. 2019, *Nature*, 575, 618, doi: [10.1038/s41586-019-1766-2](https://doi.org/10.1038/s41586-019-1766-2)
- Livio, M., & Soker, N. 1984, *Monthly Notices of the Royal Astronomical Society*, 208, 763, doi: [10.1093/mnras/208.4.763](https://doi.org/10.1093/mnras/208.4.763)
- Loeb, A., & Gaudi, B. S. 2003, *The Astrophysical Journal*, 588, L117, doi: [10.1086/375551](https://doi.org/10.1086/375551)
- Maeder, A. 1973, *A&A*, 26, 215
- Marshall, D. J., Robin, A. C., Reylé, C., Schultheis, M., & Picaud, S. 2006, *Astron. Astrophys.*, 453, 635, doi: [10.1051/0004-6361:20053842](https://doi.org/10.1051/0004-6361:20053842)
- Mashian, N., & Loeb, A. 2017, *Mon. Not. R. Astron. Soc.*, 470, doi: [10.1093/mnras/stx1410](https://doi.org/10.1093/mnras/stx1410)
- Masuda, K., & Hotokezaka, K. 2019, *Astrophys. J.*, 883, 169, doi: [10.3847/1538-4357/ab3a4f](https://doi.org/10.3847/1538-4357/ab3a4f)
- Mazeh, T., Goldberg, D., Duquenois, A., & Mayor, M. 1992, *ApJ*, 401, 265, doi: [10.1086/172058](https://doi.org/10.1086/172058)
- McCullough, P. R., Stys, J. E., Valenti, J. A., et al. 2005, *Publications of the Astronomical Society of the Pacific*, 117, 783, doi: [10.1086/432024](https://doi.org/10.1086/432024)
- Meurer, A., Smith, C. P., Paprocki, M., et al. 2017, *PeerJ Computer Science*, 3, e103, doi: [10.7717/peerj-cs.103](https://doi.org/10.7717/peerj-cs.103)
- Moe, M., & Stefano, R. D. 2017, *The Astrophysical Journal Supplement Series*, 230, 15, doi: [10.3847/1538-4365/aa6fb6](https://doi.org/10.3847/1538-4365/aa6fb6)
- Morris, S. 1985, *ApJ*, 295, 143, doi: [10.1086/163359](https://doi.org/10.1086/163359)
- Morris, S. L., & Naftilan, S. A. 1993, *ApJ*, 419, 344, doi: [10.1086/173488](https://doi.org/10.1086/173488)
- Morton, T. D. 2015, *isochrones: Stellar model grid package*, <http://ascl.net/1503.010>
- Mróz, P., Udalski, A., & Gould, A. 2022, *The Astrophysical Journal Letters*, 937, L24, doi: [10.3847/2041-8213/ac90bb](https://doi.org/10.3847/2041-8213/ac90bb)
- Nagarajan, P., El-Badry, K., Rodriguez, A. C., van Roestel, J., & Roulston, B. 2023, *Monthly Notices of the Royal Astronomical Society*, 524, 4367, doi: [10.1093/mnras/stad2130](https://doi.org/10.1093/mnras/stad2130)
- Nie, J. D., Wood, P. R., & Nicholls, C. P. 2017, *The Astrophysical Journal*, 835, 209, doi: [10.3847/1538-4357/835/2/209](https://doi.org/10.3847/1538-4357/835/2/209)
- Olejak, A., Belczynski, K., Bulik, T., & Sobolewska, M. 2020, *A&A*, 638, A94, doi: [10.1051/0004-6361/201936557](https://doi.org/10.1051/0004-6361/201936557)
- Patton, R. A., & Sukhbold, T. 2020, *MNRAS*, 499, 2803, doi: [10.1093/mnras/staa3029](https://doi.org/10.1093/mnras/staa3029)
- Patton, R. A., Sukhbold, T., & Eldridge, J. J. 2022, *Monthly Notices of the Royal Astronomical Society*, 511, 903, doi: [10.1093/mnras/stab3797](https://doi.org/10.1093/mnras/stab3797)
- Pepper, J., Pogge, R. W., DePoy, D. L., et al. 2007, *Publications of the Astronomical Society of the Pacific*, 119, 923, doi: [10.1086/521836](https://doi.org/10.1086/521836)
- Pollacco, D. L., Skillen, I., Cameron, A. C., et al. 2006, *Publications of the Astronomical Society of the Pacific*, 118, 1407, doi: [10.1086/508556](https://doi.org/10.1086/508556)
- Predehl, P., Andritschke, R., Arefiev, V., et al. 2021, *A&A*, 647, A1, doi: [10.1051/0004-6361/202039313](https://doi.org/10.1051/0004-6361/202039313)
- Price-Whelan, A. M., Sipőcz, B. M., Günther, H. M., et al. 2018, *AJ*, 156, 123, doi: [10.3847/1538-3881/aabc4f](https://doi.org/10.3847/1538-3881/aabc4f)
- Price-Whelan, A. M., Lim, P. L., Earl, N., et al. 2022, *The Astrophysical Journal*, 935, 167, doi: [10.3847/1538-4357/ac7c74](https://doi.org/10.3847/1538-4357/ac7c74)
- Qian, S.-B., Liao, W.-P., & Lajús, E. F. 2008, *The Astrophysical Journal*, 687, 466, doi: [10.1086/591515](https://doi.org/10.1086/591515)
- Rahvar, S., Mehrabi, A., & Dominik, M. 2010, *Monthly Notices of the Royal Astronomical Society*, 410, 912, doi: [10.1111/j.1365-2966.2010.17490.x](https://doi.org/10.1111/j.1365-2966.2010.17490.x)
- Renzo, M., Zapartas, E., Justham, S., et al. 2023, *The Astrophysical Journal Letters*, 942, L32, doi: [10.3847/2041-8213/aca4d3](https://doi.org/10.3847/2041-8213/aca4d3)
- Repetto, S., Igoshev, A. P., & Nelemans, G. 2017, *Monthly Notices of the Royal Astronomical Society*, 467, 298, doi: [10.1093/mnras/stx027](https://doi.org/10.1093/mnras/stx027)

- Ricker, G. R., Winn, J. N., Vanderspek, R., et al. 2014, in *Space Telescopes and Instrumentation 2014: Optical, Infrared, and Millimeter Wave*, ed. J. M. O. Jr., M. Clampin, G. G. Fazio, & H. A. MacEwen, Vol. 9143, International Society for Optics and Photonics (SPIE), 556 – 570. <https://doi.org/10.1117/12.2063489>
- Rimoldini, Lorenzo, Holl, Berry, Gavras, Panagiotis, et al. 2023, *A&A*, 674, A14, doi: [10.1051/0004-6361/202245591](https://doi.org/10.1051/0004-6361/202245591)
- Rivinius, Th., Baade, D., Hadrava, P., Heida, M., & Klement, R. 2020, *A&A*, 637, L3, doi: [10.1051/0004-6361/202038020](https://doi.org/10.1051/0004-6361/202038020)
- Romani, R. W., Kandel, D., Filippenko, A. V., Brink, T. G., & Zheng, W. 2022, *The Astrophysical Journal Letters*, 934, L17, doi: [10.3847/2041-8213/ac8007](https://doi.org/10.3847/2041-8213/ac8007)
- Rowan, D. M., Stanek, K. Z., Jayasinghe, T., et al. 2021, *Monthly Notices of the Royal Astronomical Society*, 507, 104, doi: [10.1093/mnras/stab2126](https://doi.org/10.1093/mnras/stab2126)
- Sahu, K. C., Anderson, J., Casertano, S., et al. 2022, *The Astrophysical Journal*, 933, 83, doi: [10.3847/1538-4357/ac739e](https://doi.org/10.3847/1538-4357/ac739e)
- Sanderson, R. E., Wetzel, A., Loebman, S., et al. 2020, *Astrophys. J. Suppl. Ser.*, 246, doi: [10.3847/1538-4365/ab5b9d](https://doi.org/10.3847/1538-4365/ab5b9d)
- Saracino, S., Kamann, S., Guarcello, M. G., et al. 2021, *Monthly Notices of the Royal Astronomical Society*, 511, 2914, doi: [10.1093/mnras/stab3159](https://doi.org/10.1093/mnras/stab3159)
- Sartoretti, P., Marchal, O., Babusiaux, C., et al. 2023, *A&A*, 674, A6, doi: [10.1051/0004-6361/202243615](https://doi.org/10.1051/0004-6361/202243615)
- Shahaf, S., Bashi, D., Mazeh, T., et al. 2022, *Monthly Notices of the Royal Astronomical Society*, 518, 2991, doi: [10.1093/mnras/stac3290](https://doi.org/10.1093/mnras/stac3290)
- Shahaf, S., Hallakoun, N., Mazeh, T., et al. 2023, *arXiv e-prints*, arXiv:2309.15143, doi: [10.48550/arXiv.2309.15143](https://doi.org/10.48550/arXiv.2309.15143)
- Shahaf, S., Mazeh, T., Faigler, S., & Holl, B. 2019, *Monthly Notices of the Royal Astronomical Society*, 487, 5610, doi: [10.1093/mnras/stz1636](https://doi.org/10.1093/mnras/stz1636)
- Shakura, N. I., & Postnov, K. A. 1987, *A&A*, 183, L21
- Shappee, B. J., Prieto, J. L., Grupe, D., et al. 2014, *The Astrophysical Journal*, 788, 48, doi: [10.1088/0004-637x/788/1/48](https://doi.org/10.1088/0004-637x/788/1/48)
- Shenar, T., Sana, H., Mahy, L., et al. 2022a, *Nature Astronomy*, 6, 1085, doi: [10.1038/s41550-022-01730-y](https://doi.org/10.1038/s41550-022-01730-y)
- . 2022b, *A&A*, 665, A148, doi: [10.1051/0004-6361/202244245](https://doi.org/10.1051/0004-6361/202244245)
- Shikauchi, M., Tsuna, D., Tanikawa, A., & Kawanaka, N. 2023, *The Astrophysical Journal*, 953, 52, doi: [10.3847/1538-4357/acd752](https://doi.org/10.3847/1538-4357/acd752)
- Shporer, A. 2017, *Publications of the Astronomical Society of the Pacific*, 129, 072001, doi: [10.1088/1538-3873/aa7112](https://doi.org/10.1088/1538-3873/aa7112)
- Simpson, E. R., Fetherolf, T., Kane, S. R., et al. 2022, *The Astronomical Journal*, 163, 215, doi: [10.3847/1538-3881/ac5d41](https://doi.org/10.3847/1538-3881/ac5d41)
- Soubiran, C., Jasiewicz, G., Chemin, L., et al. 2018, *A&A*, 616, A7, doi: [10.1051/0004-6361/201832795](https://doi.org/10.1051/0004-6361/201832795)
- Stassun, K. G., Oelkers, R. J., Pepper, J., et al. 2018, *AJ*, 156, 102, doi: [10.3847/1538-3881/aad050](https://doi.org/10.3847/1538-3881/aad050)
- Sullivan, P. W., Winn, J. N., Berta-Thompson, Z. K., et al. 2015, *Astrophys. J.*, 809, 77, doi: [10.1088/0004-637X/809/1/77](https://doi.org/10.1088/0004-637X/809/1/77)
- Sweeney, D., Tuthill, P., Sharma, S., & Hirai, R. 2022, *MNRAS*, 516, 4971, doi: [10.1093/mnras/stac2092](https://doi.org/10.1093/mnras/stac2092)
- Tanikawa, A., Hattori, K., Kawanaka, N., et al. 2023, *The Astrophysical Journal*, 946, 79, doi: [10.3847/1538-4357/acbf36](https://doi.org/10.3847/1538-4357/acbf36)
- Thompson, S. E., Everett, M., Mullally, F., et al. 2012, *The Astrophysical Journal*, 753, 86, doi: [10.1088/0004-637x/753/1/86](https://doi.org/10.1088/0004-637x/753/1/86)
- Thompson, T. A., Kochanek, C. S., Stanek, K. Z., et al. 2019, *Science* (80-.), 366, 637, doi: [10.1126/science.aau4005](https://doi.org/10.1126/science.aau4005)
- Tomsick, J. A., & Muterspaugh, M. W. 2010, *The Astrophysical Journal*, 719, 958, doi: [10.1088/0004-637x/719/1/958](https://doi.org/10.1088/0004-637x/719/1/958)
- Tout, C. A., Aarseth, S. J., Pols, O. R., & Eggleton, P. P. 1997, *MNRAS*, 291, 732, doi: [10.1093/mnras/291.4.732](https://doi.org/10.1093/mnras/291.4.732)
- Trimble, V. L., & Thorne, K. S. 1969, *ApJ*, 156, 1013, doi: [10.1086/150032](https://doi.org/10.1086/150032)
- van de Kamp, P. 1975, *ARA&A*, 13, 295, doi: [10.1146/annurev.aa.13.090175.001455](https://doi.org/10.1146/annurev.aa.13.090175.001455)
- van den Heuvel, E. P. J., & Tauris, T. M. 2020, *Science*, 368, eaba3282, doi: [10.1126/science.aba3282](https://doi.org/10.1126/science.aba3282)
- van der Walt, S., Colbert, S. C., & Varoquaux, G. 2011, *Computing in Science and Engineering*, 13, 22, doi: [10.1109/MCSE.2011.37](https://doi.org/10.1109/MCSE.2011.37)
- van Kerkwijk, M. H., Rappaport, S. A., Breton, R. P., et al. 2010, *The Astrophysical Journal*, 715, 51, doi: [10.1088/0004-637x/715/1/51](https://doi.org/10.1088/0004-637x/715/1/51)
- Virtanen, P., Gommers, R., Oliphant, T. E., et al. 2020, *Nature Methods*, 17, 261, doi: [10.1038/s41592-019-0686-2](https://doi.org/10.1038/s41592-019-0686-2)
- Webbink, R. F. 1985, in *Interacting Binary Stars*, ed. J. E. Pringle & R. A. Wade, 39
- Wes McKinney. 2010, in *Proceedings of the 9th Python in Science Conference*, ed. Stéfan van der Walt & Jarrod Millman, 56 – 61

- Wetzel, A. R., Hopkins, P. F., Kim, J.-h., et al. 2016, *Astrophys. J.*, 827, L23, doi: [10.3847/2041-8205/827/2/l23](https://doi.org/10.3847/2041-8205/827/2/l23)
- Wiktorowicz, G., Middleton, M., Khan, N., et al. 2021, *Monthly Notices of the Royal Astronomical Society*, 507, 374, doi: [10.1093/mnras/stab2135](https://doi.org/10.1093/mnras/stab2135)
- Wiktorowicz, G., Wyrzykowski, L., Chruslinska, M., et al. 2019, *Astrophys. J.*, 885, 1, doi: [10.3847/1538-4357/ab45e6](https://doi.org/10.3847/1538-4357/ab45e6)
- Witt, H. J., & Mao, S. 1994, *ApJ*, 430, 505, doi: [10.1086/174426](https://doi.org/10.1086/174426)
- Zeipel, H. v. 1924, *Monthly Notices of the Royal Astronomical Society*, 84, 665, doi: [10.1093/mnras/84.9.665](https://doi.org/10.1093/mnras/84.9.665)
- Zeldovich, Y. B., & Guseynov, O. H. 1966, *ApJ*, 144, 840, doi: [10.1086/148672](https://doi.org/10.1086/148672)
- Zhao, X., Wang, S., Li, X., et al. 2023, arXiv e-prints, arXiv:2308.03255, doi: [10.48550/arXiv.2308.03255](https://doi.org/10.48550/arXiv.2308.03255)
- Zucker, S., Mazeh, T., & Alexander, T. 2007, *The Astrophysical Journal*, 670, 1326, doi: [10.1086/521389](https://doi.org/10.1086/521389)

APPENDIX

A. SUPPLIMENTARY FIGURES

Here we present selected results from our **delayed** model. [Figure A3](#) shows the detection fraction as a function of P_{orb} for the **delayed** model for our detected population of BH-LC binaries. The detection fraction in the **delayed** model is very similar to the same for the **rapid** model ([Figure 10](#)). [Figure A1](#) and [A4](#) shows the set diagram for the **delayed** model. [Figure A2](#) shows the detection fraction as a function of M_{BH} for $\text{SNR} \geq 1, 5$ and 10 .

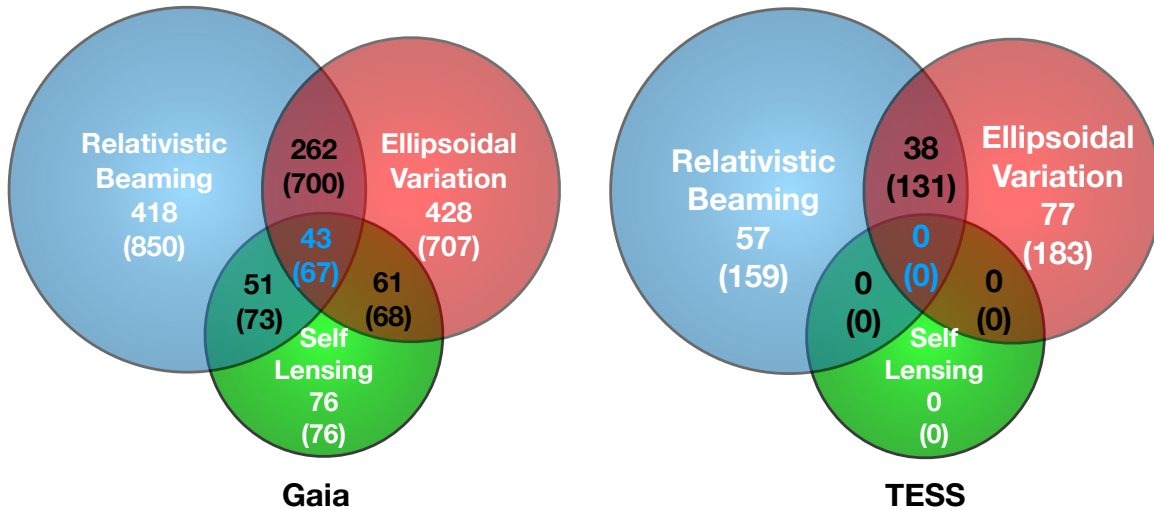


Figure A1. Same as [Figure 3](#) but for the BH-LCs in our **delayed** model.

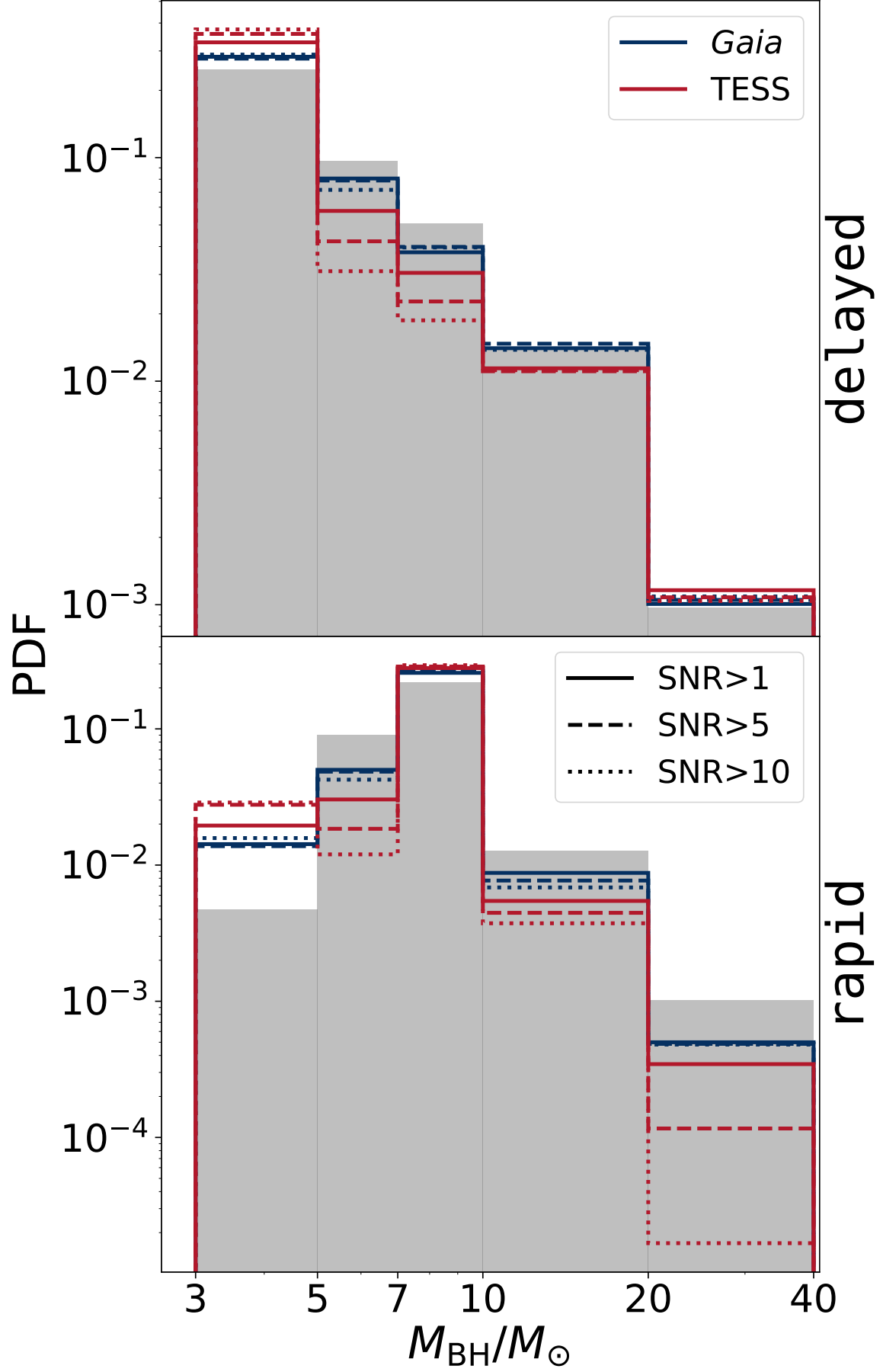


Figure A2. Same as the top panel of Figure 4 but includes BH-LC binaries with $\text{SNR} \geq 1$ (solid), 5 (dashed), and 10 (dotted).

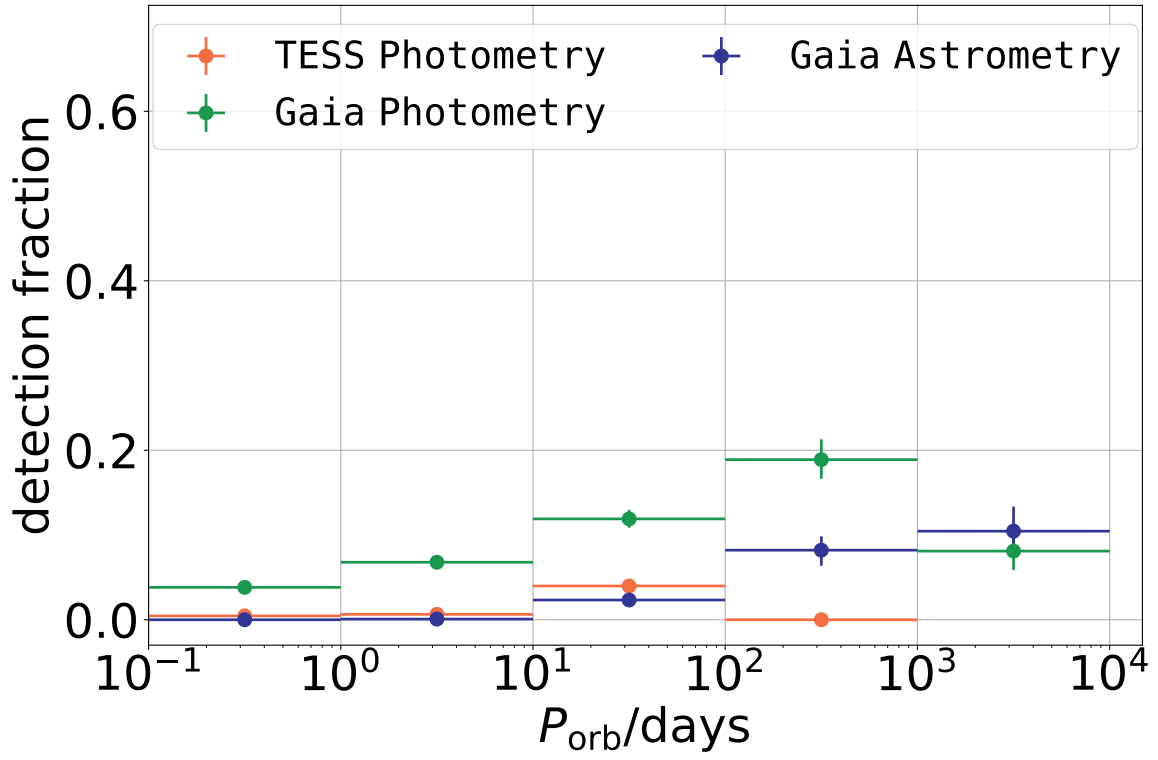


Figure A3. Same as Figure 10 but for the BH-LCs in our delayed model.

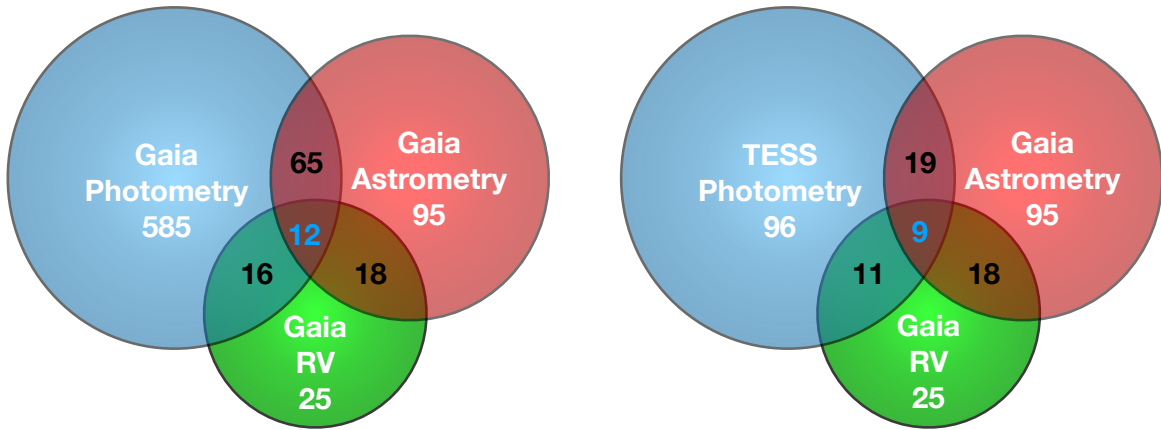


Figure A4. Same as Figure 11 but for the BH-LCs in our delayed model.